Supporting Information

A water playground for peptide re-assembly from fibrils to plates

Simone Adorinni,[a] Marina Kurbasic,[a] Ana M. Garcia,[a,b] Slavko Kralj,[c,d] Ottavia Bellotto,[a] Erica Scarel,[a] Paolo Pengo,[a] Rita De Zorzi,[a] Michele Melchionna,[a] Attilio V. Vargiu*[e] and Silvia Marchesan*[a]

[a] Department of Chemical and Pharmaceutical Sciences, University of Trieste, Via . Giorgieri 1, 34127 Trieste, Italy
E-mail: smarchesan@units.it
[b] Facultad de Ciencias y Tecnologías Químicas, Instituto Regional de Investigación Científica Aplicada (IRICA), Universidad de Castilla-La Mancha, Ciudad Real 13071, Spain
[c] Materials Synthesis Department, Jožef Stefan Institute, Jamova 39, 1000 Ljubljana, Slovenia
[d] Department of Pharmaceutical Technology, Faculty of Pharmacy, University of Ljubljana 1000 Ljubljana, Slovenia
[e] Department of Physics, University of Cagliari, Cittadella Universitaria, S.P. 8 km. 0.7, 09042 Monserrato (CA), Italy
E-mail: vargiu@dsf.unica.it

Table of Contents

S1. ^{D}Nle-^{D}Leu-^{L}Phe-^{L}Phe spectroscopic data

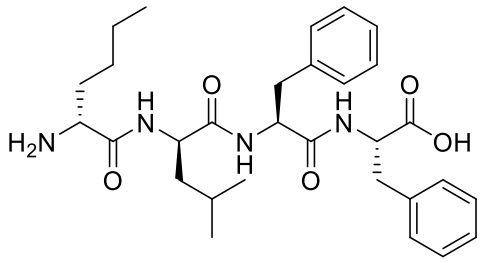

^{1}H-NMR (400 MHz, DMSO-d_6) δ (ppm) 12.75 (s (br), 1H, -COOH), 8.38 (d, *J* = 8.0 Hz, 1H, NH), 8.35 (d, *J* = 4.4 Hz, 1H, NH), 8.33 (d, *J* = 4.8 Hz, 1H, NH) 8.00 (s, 2H, NH_2), 7.29-7.14 (m, 10H, Ar), 4.63-4.58 (ddd, *J* = 15.7, 8.0, 4.0 Hz, 1H, αCH Phe_3), 4.43 (dd, *J* = 8.2, 5.6 Hz, 1H, αCH), 4.33 (dd, *J* = 15.7, 7.6 Hz, 1H, αCH), 3.67 (dd, *J* = 11.8, 5.8 Hz, 1H, αCH), 3.07-2.99 (m, 2H, βCH), 2.91 (dd, *J* = 14.0, 8.5 Hz 1H, βCH), 2.65 (dd, *J* = 13.5, 11.4 Hz, 1H, βCH), 1.59-1.55 (m, 2H, βCH), 1.38-1.12 (m, 5H, β and γ CH), 1.02 (m, 2H, γ CH), 0.85 (t, *J* = 7.2 Hz, 3H, γ CH), 0.70 (m, 5H, δ and ε CH).

^{13}C NMR (100 MHz, DMSO-d_6) δ (ppm) 173.1, 171.8, 171.4, 168.6 (4 x CO); 138.2, 137.9, 129.8, 129.5, 128.6, 128.3, 126.9, 126.6, 126.0 ,125.0 (Ar); 54.1, 54.0, 52.5, 51.2 (4 x αC); 41.9, 38.5, 38.2, 37.2 (4 x βC), 31.4, 26.6 (2 x γC), 24.2, 23.2, 22.2 (3 x δC), 14.1 (εC).

HR-MS (ESI): m/z 539.3227 $(M+H)^+$ $C_{30}H_{43}N_4O_5$ requires 539.3228.

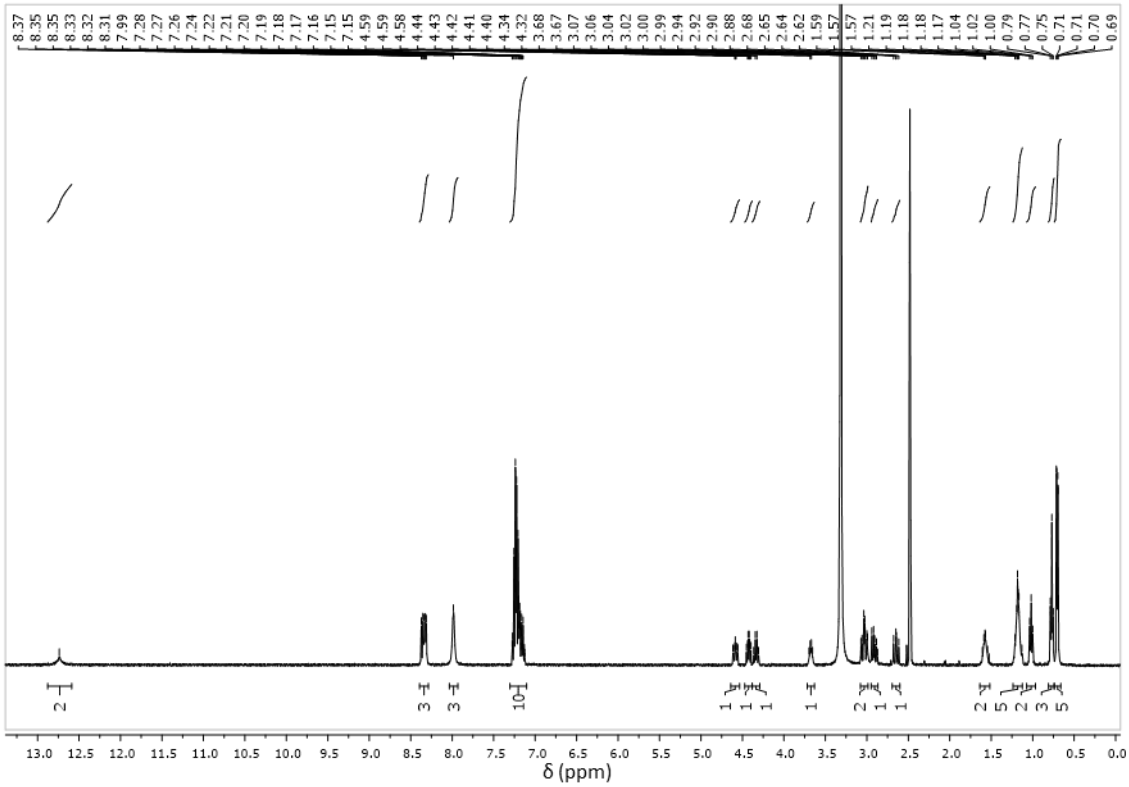

Fig. S1. ^{1}H-NMR spectrum of ^{D}Nle-^{D}Leu-^{L}Phe-^{L}Phe.

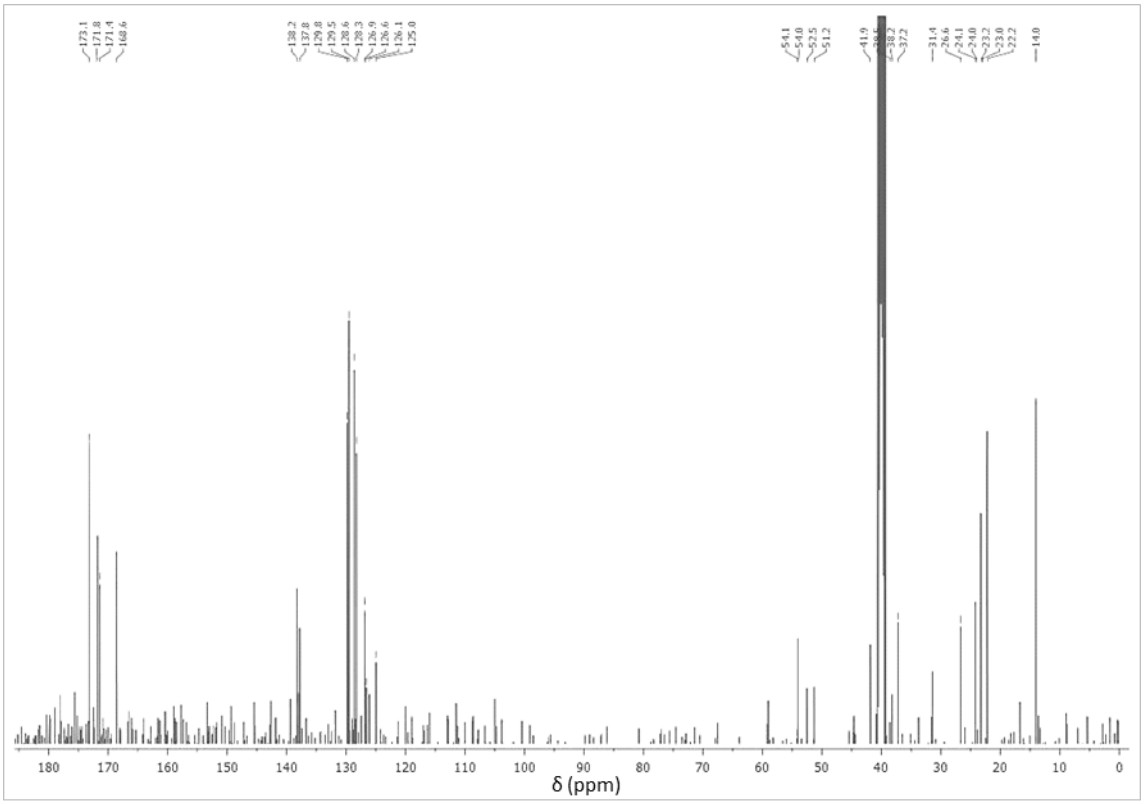

Fig. S2. ^{13}C-NMR spectrum of ^{D}Nle-^{D}Leu-^{L}Phe-^{L}Phe.

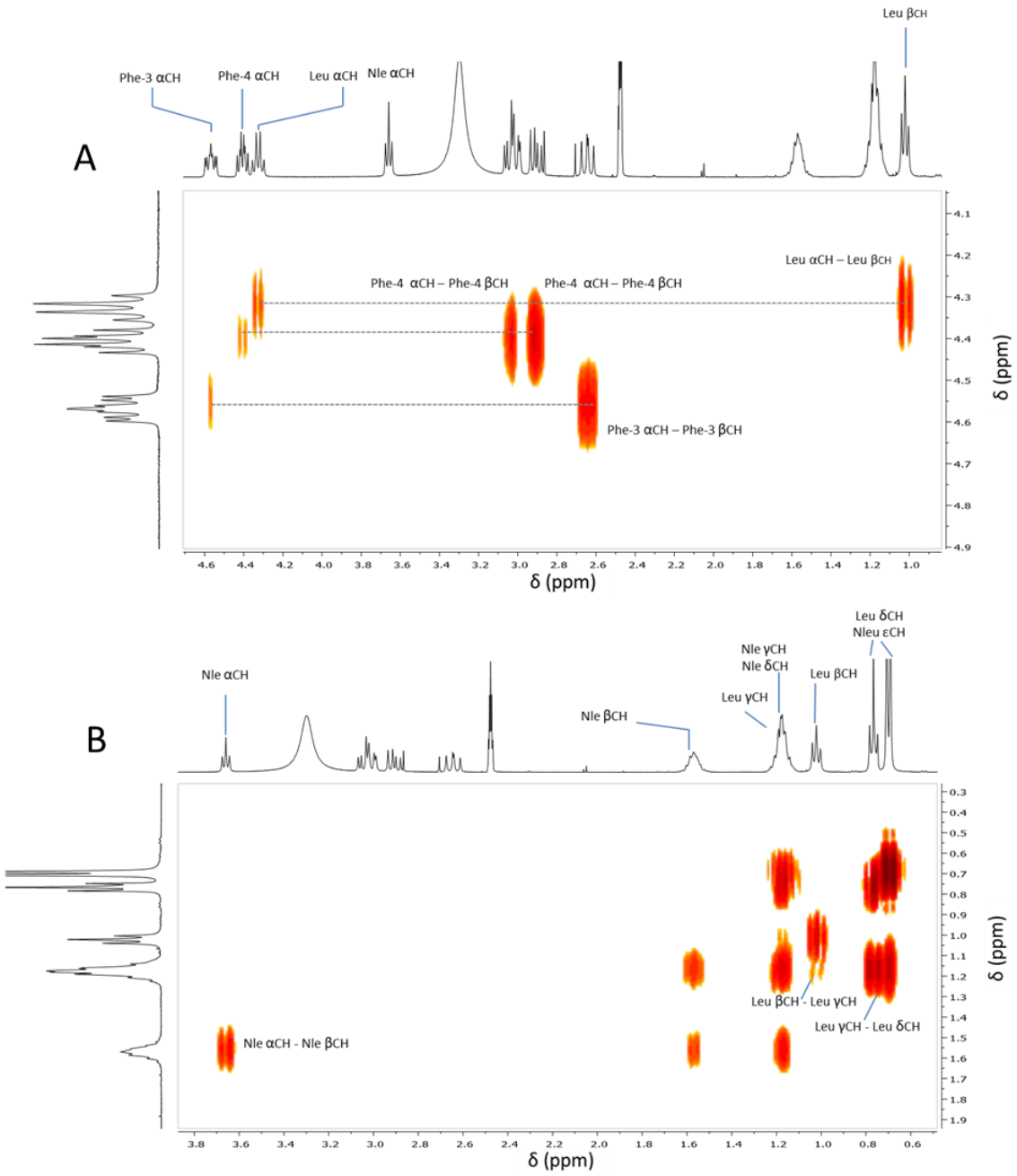

Fig. S3. gCOSY spectrum of ^{D}Nle-^{D}Leu-^{L}Phe-^{L}Phe.

A α and β proton correlation, **B** aliphatic proton correlation.

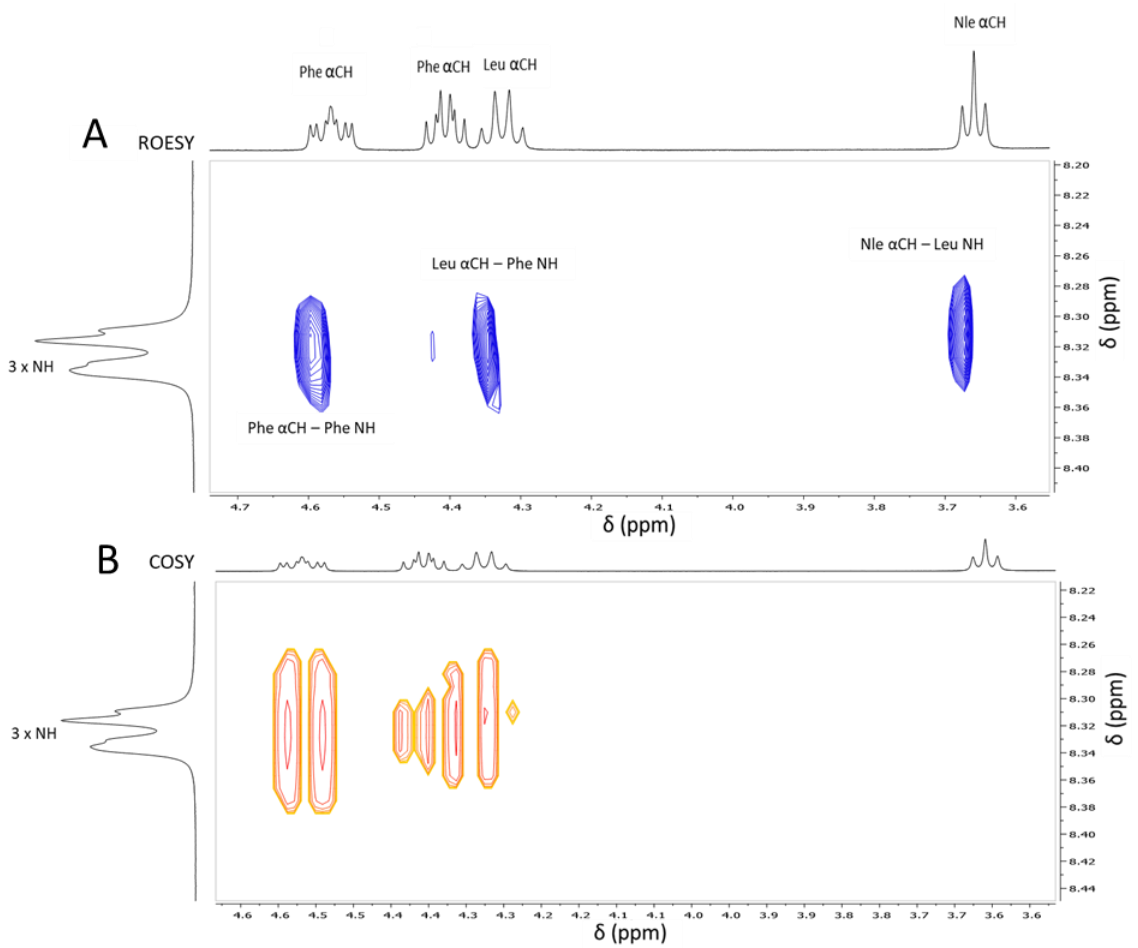

Fig. S4. gROESY (**A**) and gCOSY (**B**) NMR spectrum of ^{D}Nle-^{D}Leu-^{L}Phe-^{L}Phe.

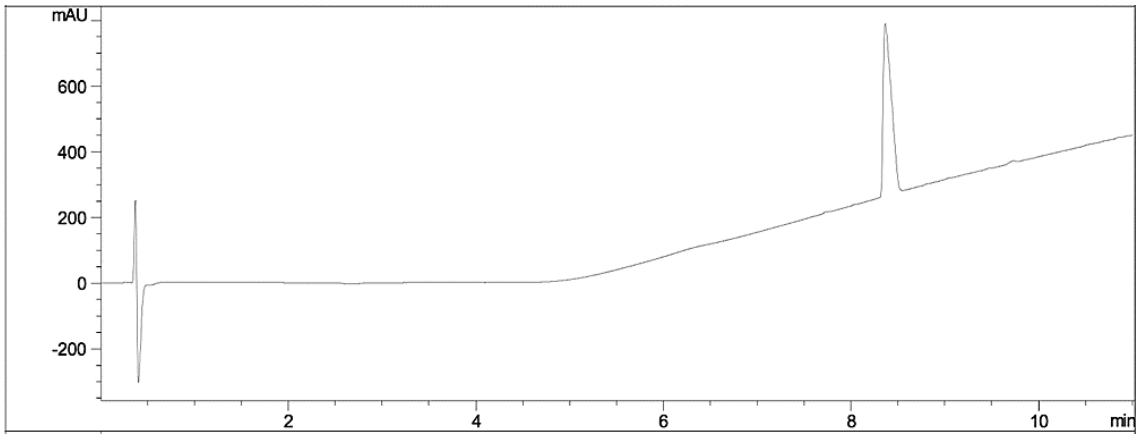

Fig. S5. HPLC trace of ^{D}Nle-^{D}Leu-^{L}Phe-^{L}Phe (Abs @ 214 nm).

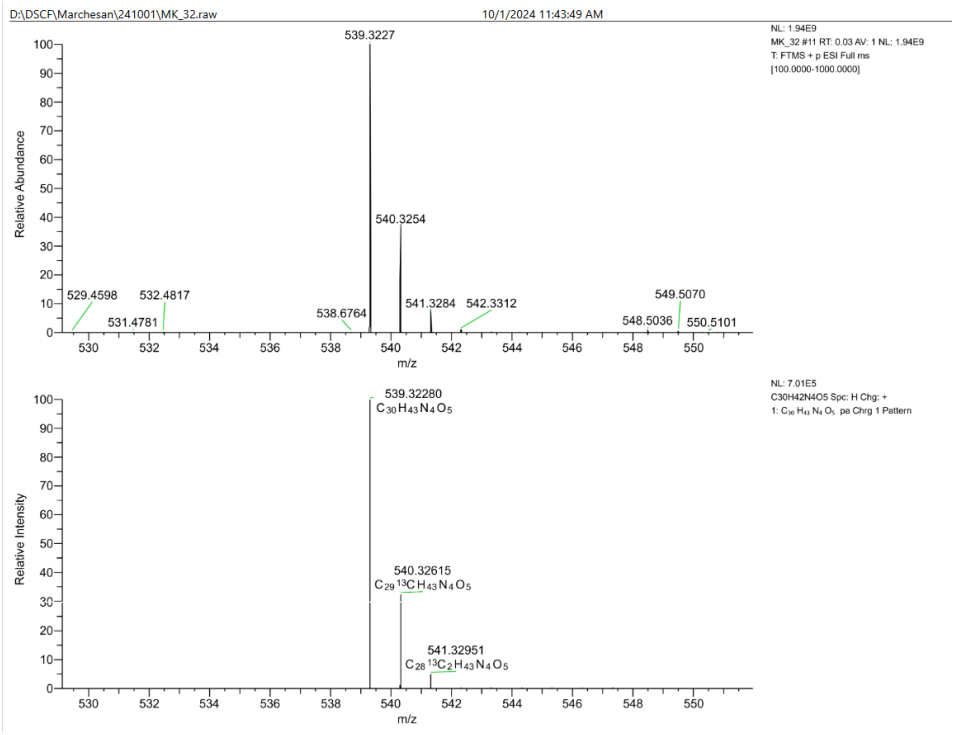

Fig. S6. HR-MS experimental (top) and theoretical (bottom) spectrum of ^{D}Nle-^{D}Leu-^{L}Phe-^{L}Phe.

S2. ^{L}Nle-^{L}Leu-^{L}Phe-^{L}Phe spectroscopic data

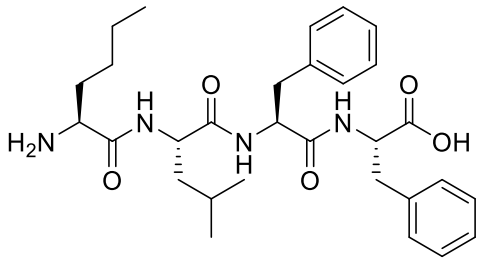

^{1}H-NMR (400 MHz, DMSO-d_6) δ (ppm) 8.34 (d, *J*=8.4 Hz, 1H, NH), 8.23 (d, *J*=7.7 Hz, 1H, NH), 8.07(d, *J*=8.3 Hz, 3H, NH), 7.41-6.94 (m, 10H, Ar), 4.53 (dd, *J*=8.3, 5.4 Hz, 1H, αCH), 4.41 (dd, *J* = 8.3, 5.4 Hz, 1H, αCH), 4.33 (dd, *J* = 15.5, 7.7 Hz, 1H, αCH), 3.66 (dd, *J* = 6.4 Hz, 1H, αCH), 3.07-2.85 (m, 3H, β CH), 2.79-2.69 (m, 1H, βCH), 1.63-1.46 (m, 3H, β and γ CH), 1.34 (t, *J* = 7.3 Hz, 2H, βCH), 1.26-1.08 (m, 5H, γ and δ CH), 0.85-0.77 (m, 8H, δ and ε CH).

^{13}C NMR (101 MHz, DMSO-d_6) δ (ppm) 173.1, 171.6, 171.3, 168.7 (4 x CO); 138.0, 137.8, 129.5, 129.5, 128.6, 128.3, 126.9, 126.6, 126.5, 124.5 (10 x Ar); 53.9, 53.7, 52.5, 51.4 (4 x αC); 41.6, 37.9, 37.1, 37.1 (4 x βC), 31.2, 26.5 (2 x γC), 24.4, 23.5, 22.2 (3 x δC), 14.1 (εC).

HR-MS (ESI): m/z 539.3227 $(M+H)^+$ $C_{30}H_{43}N_4O_5$ requires 539.3228.

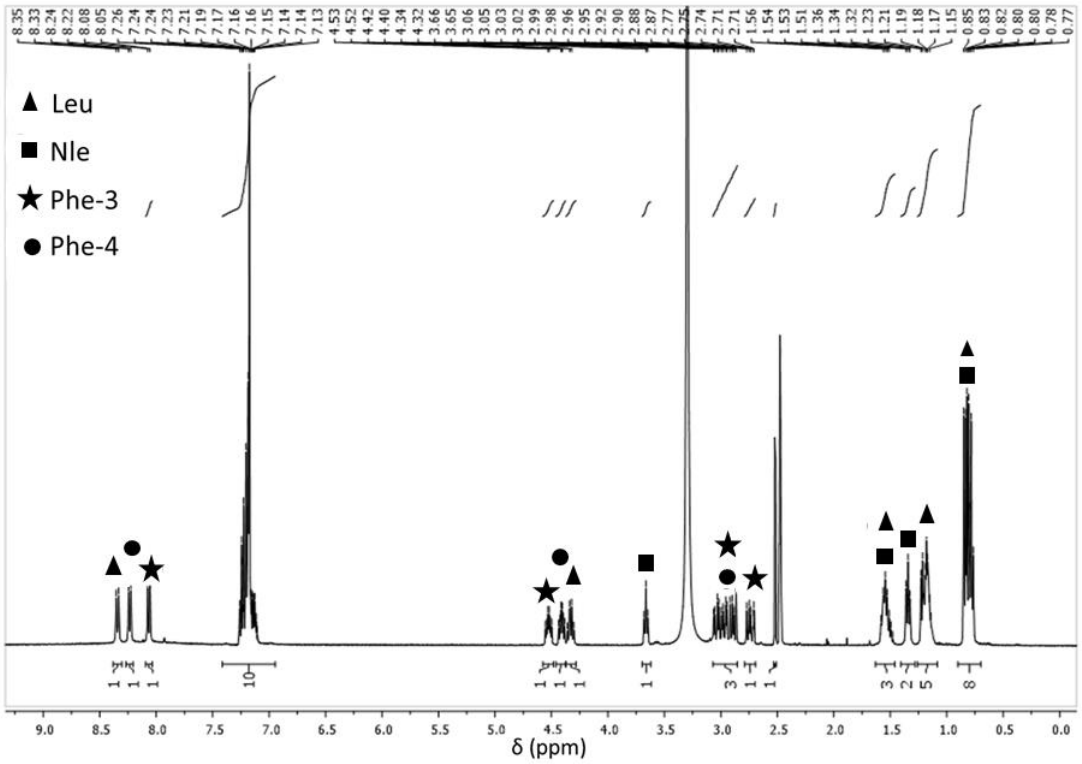

Fig. S7. ^{1}H-NMR spectrum of ^{L}Nle-^{L}Leu-^{L}Phe-^{L}Phe.

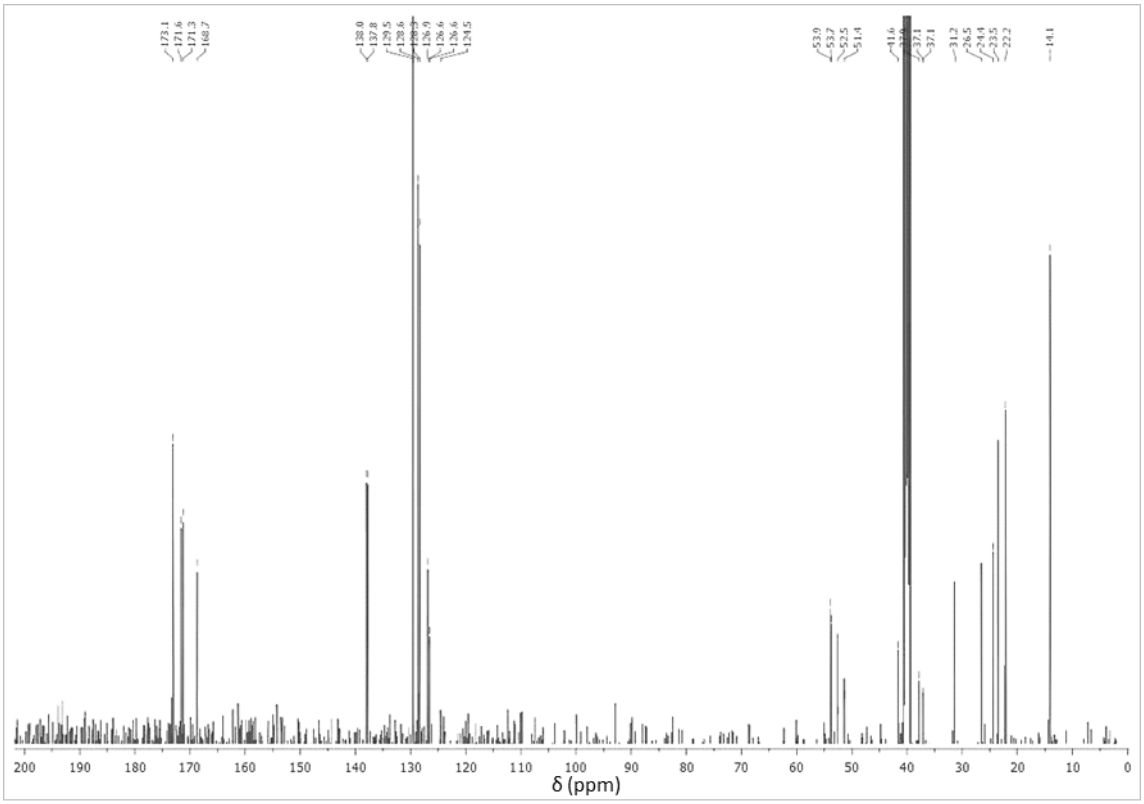

Fig. S8. ^{13}C-NMR spectrum of ^{L}Nle-^{L}Leu-^{L}Phe-^{L}Phe.

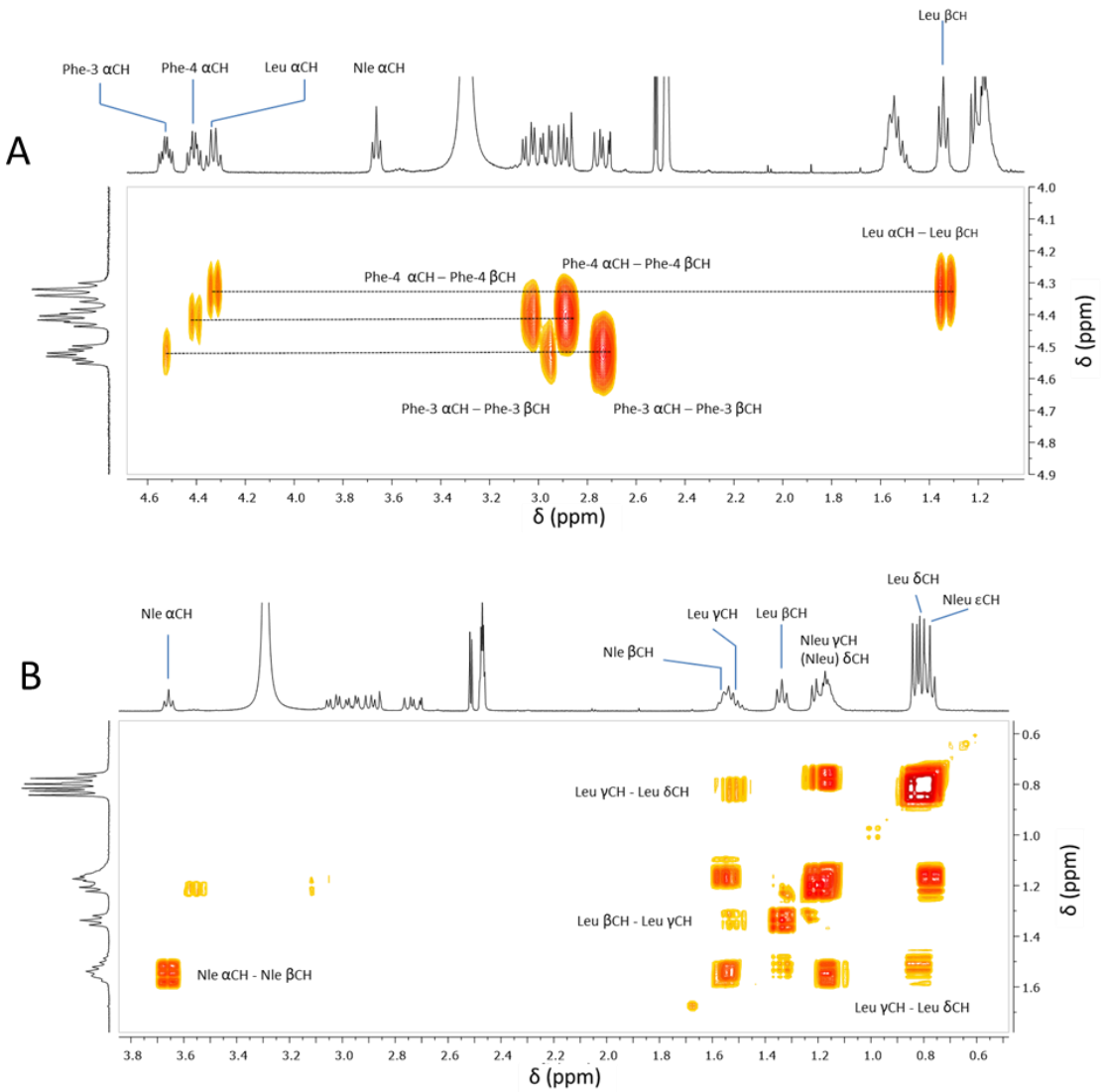

Fig. S9. gCOSY spectrum of ^{L}Nle-^{L}Leu-^{L}Phe-^{L}Phe correlation.

A α and β proton correlation, **B** aliphatic proton correlation.

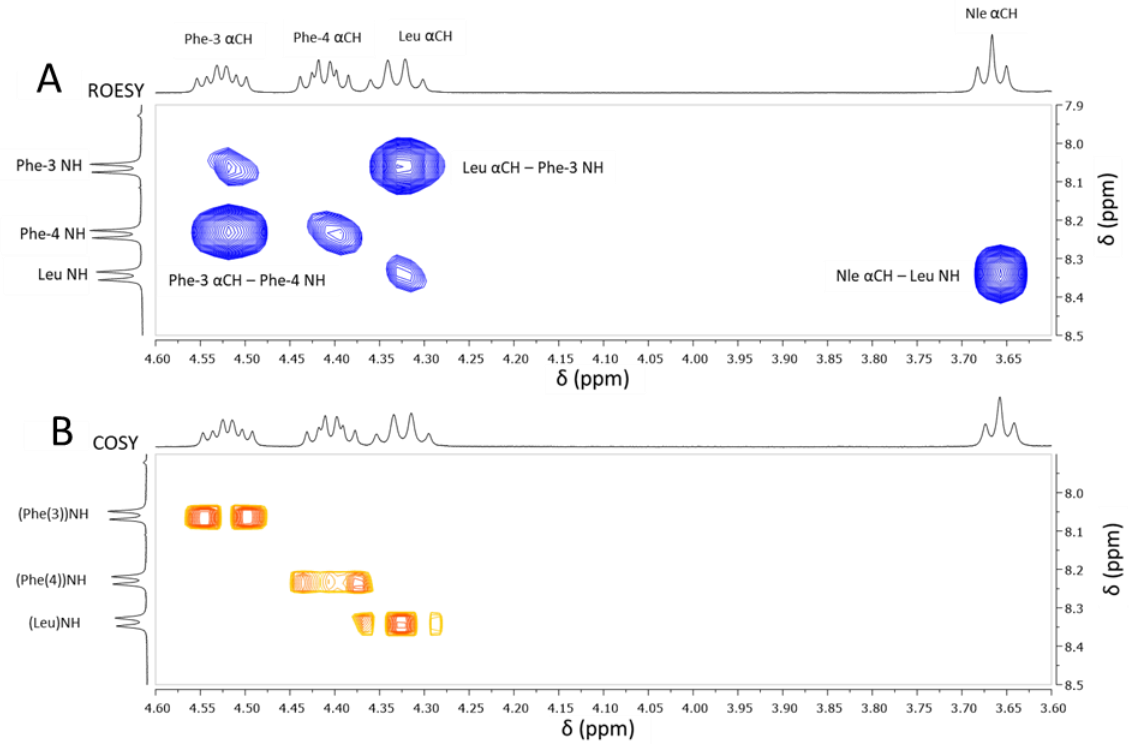

Fig. S10. gROESY (**A**) and gCOSY (**B**) NMR spectrum of ^{D}Nle-^{D}Leu-^{L}Phe-^{L}Phe.

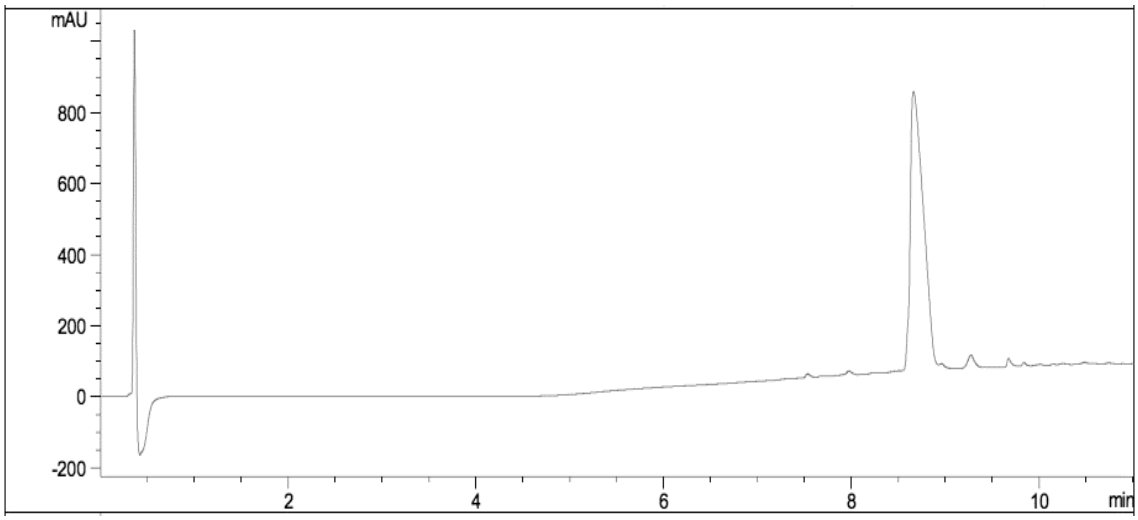

Fig. S11. HPLC trace of ^{L}Nle-^{L}Leu-^{L}Phe-^{L}Phe (Abs @ 214 nm).

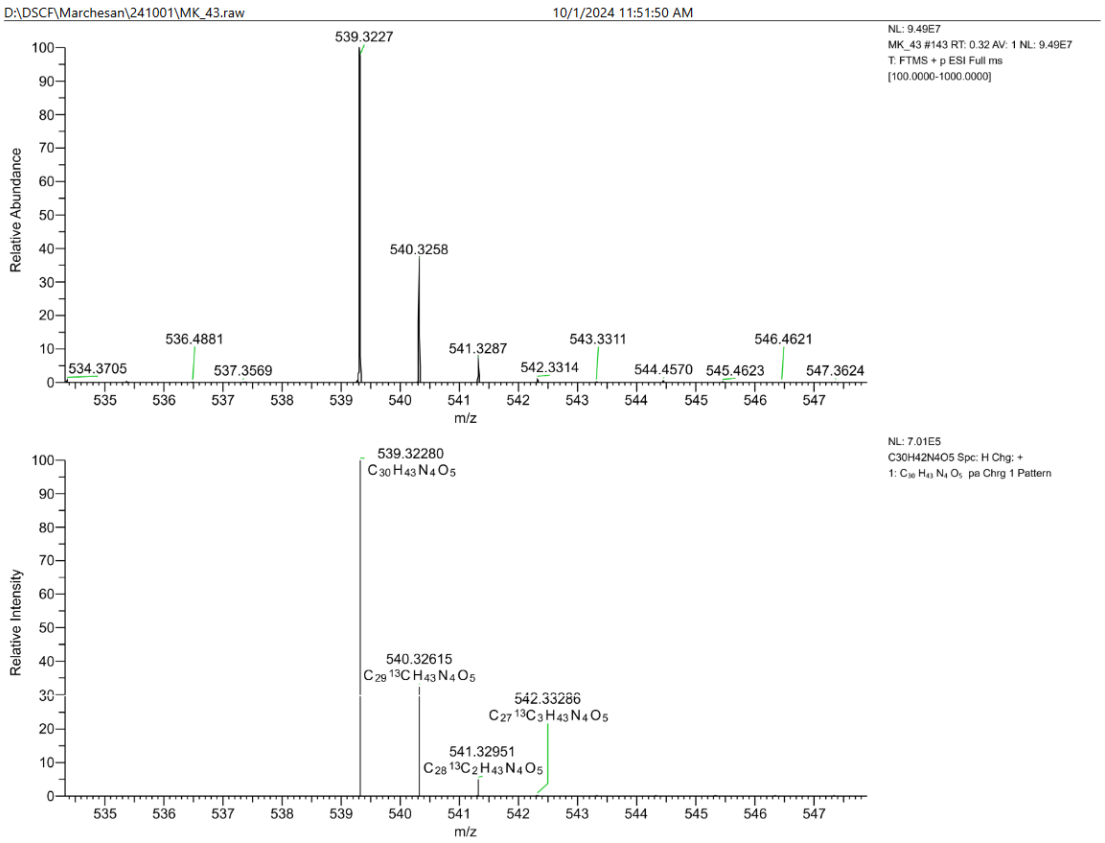

Fig. S12. HR-MS experimental (top) and theoretical (bottom) spectrum of ^{L}Nle-^{L}Leu-^{L}Phe-^{L}Phe.

S3. Ac - ^{D}Leu-^{L}Phe-^{L}Phe spectroscopic data

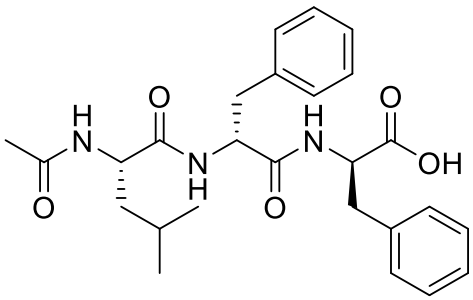

^{1}H-NMR (400 MHz, DMSO) δ (ppm) 8.23-8.21 (m, 2H, NH), 7.90 (d, *J*=7.9 Hz, 1H, NH), 7.34-7.07 (m, 10H, Ar), 4.50-4.38 (m, 2H, αCH), 4.18 (dd, *J*=15.1, 7.5 Hz,1H, αCH), 3.05-2.95 (m, 4H, βCH), 2.65 (dd, *J*= 13.7, 11.1, 1H, βCH), 1.76 (s, 3H, CH_3 – Ac.) 1.10 (m, 3H, βCH and γCH), 0.69 (dd, *J*= 12.5, 6.3 Hz, 6H, δCH).

^{13}C-NMR (101 MHz, DMSO) δ (ppm) 173.1, 172.3, 171.7, 169.6, (4 x CO); 138.4, 137.9, 129.7, 129.5, 128.7, 128.3, 127.0, 126.9 (10 x Ar); 54.1, 54.0, 51.6 (3 x αC); 41.4, 37.1, 24.3 (3 x βC);

23.1 (C-CH_3); 22.8 (γC) 22.5, (δC).

MS (ESI):m/z 467.2 $(M+H)^+C_{26}H_{33}N_3O_5$ requires 467.7.

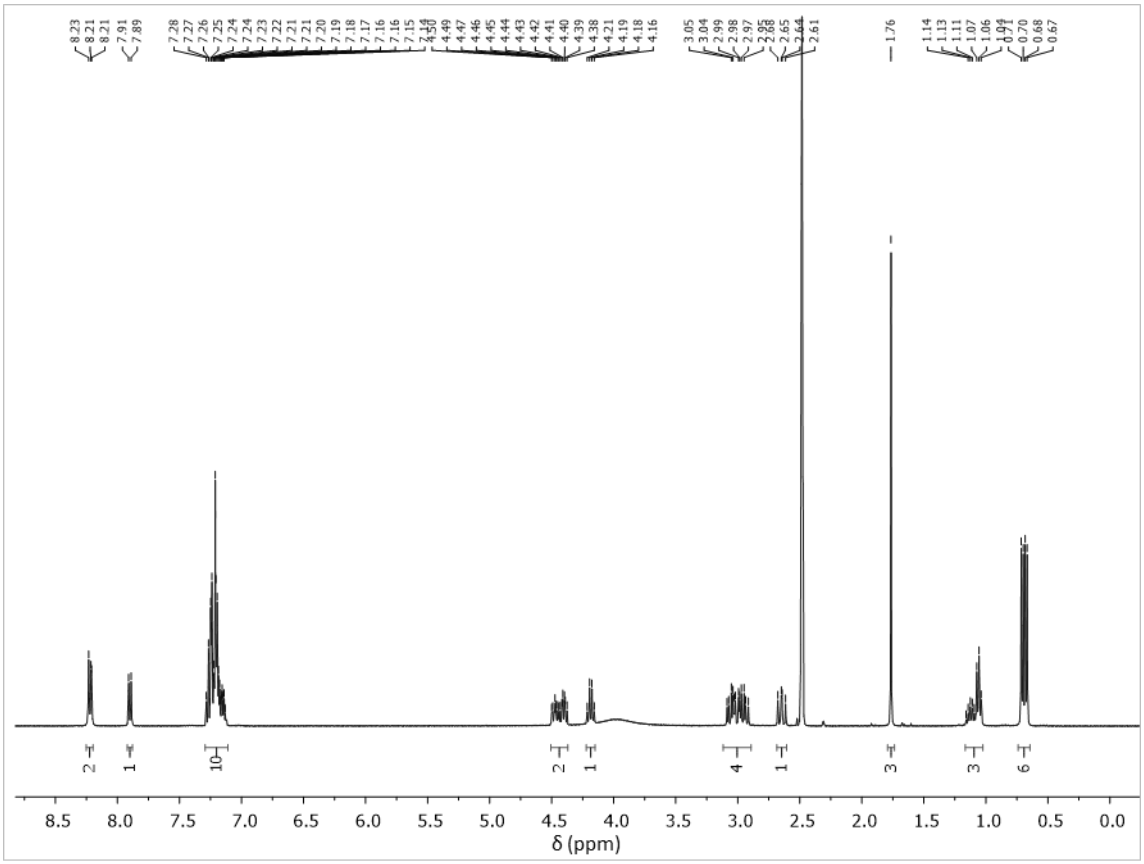

Fig. S13. ^{1}H-NMR spectrum of Ac-^{D}Leu-^{L}Phe-^{L}Phe.

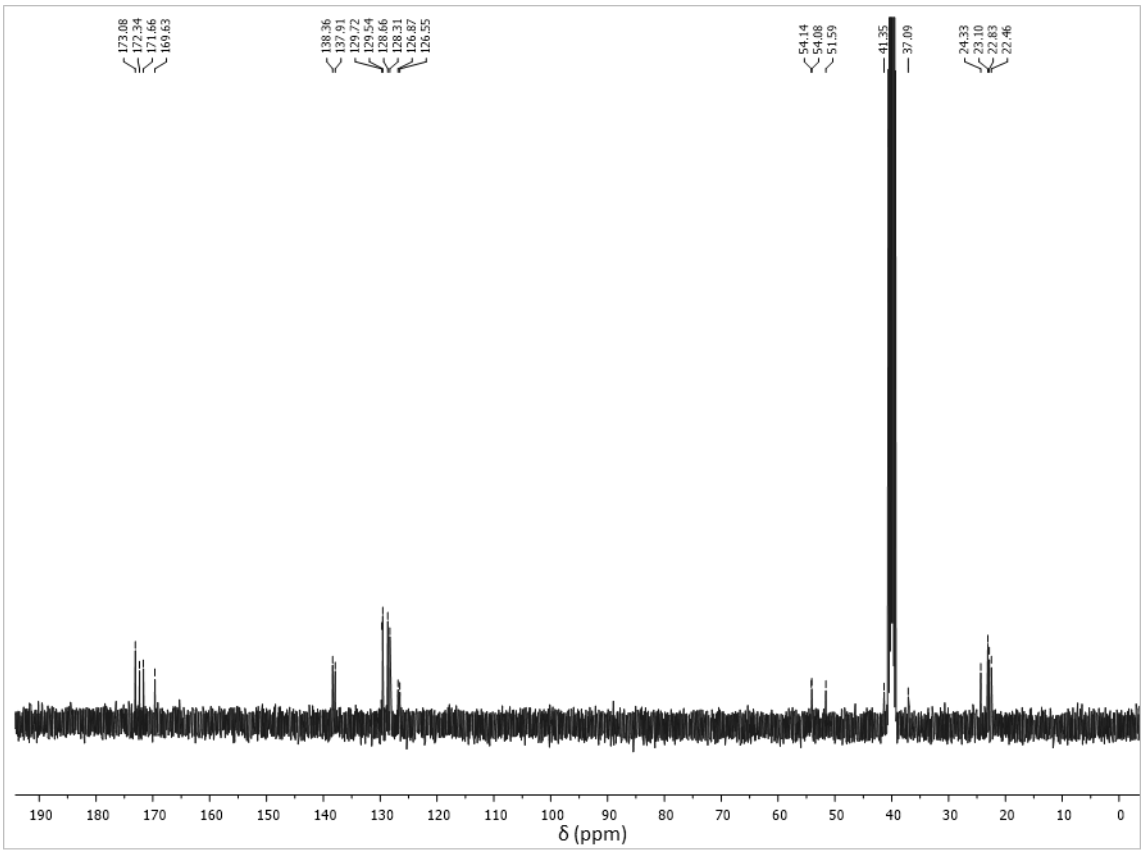

Fig. S14. ^{13}C-NMR spectrum of Ac-^{D}Leu-^{L}Phe-^{L}Phe.

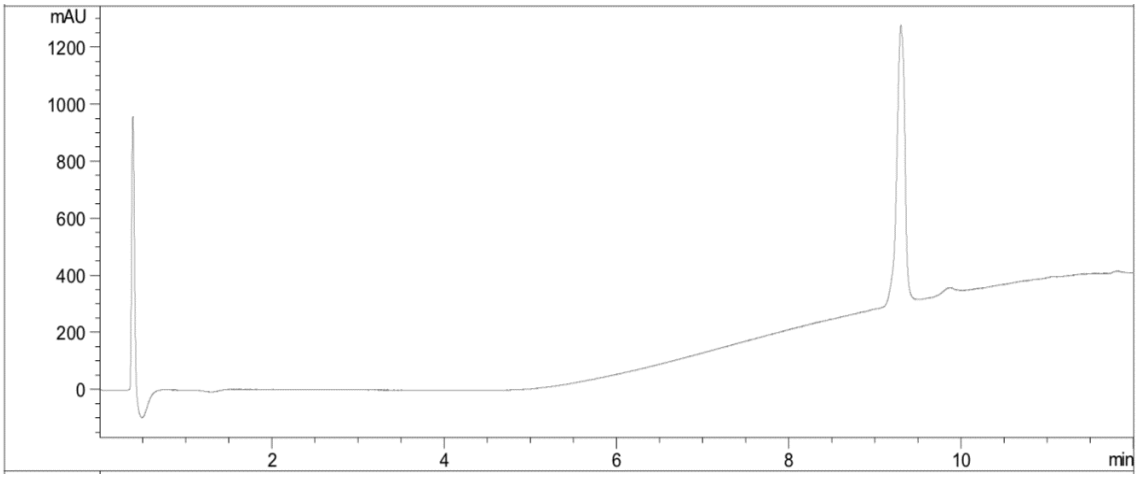

Fig. S15. HPLC trace of Ac-^{D}Leu-^{L}Phe-^{L}Phe. (Abs @ 214 nm).

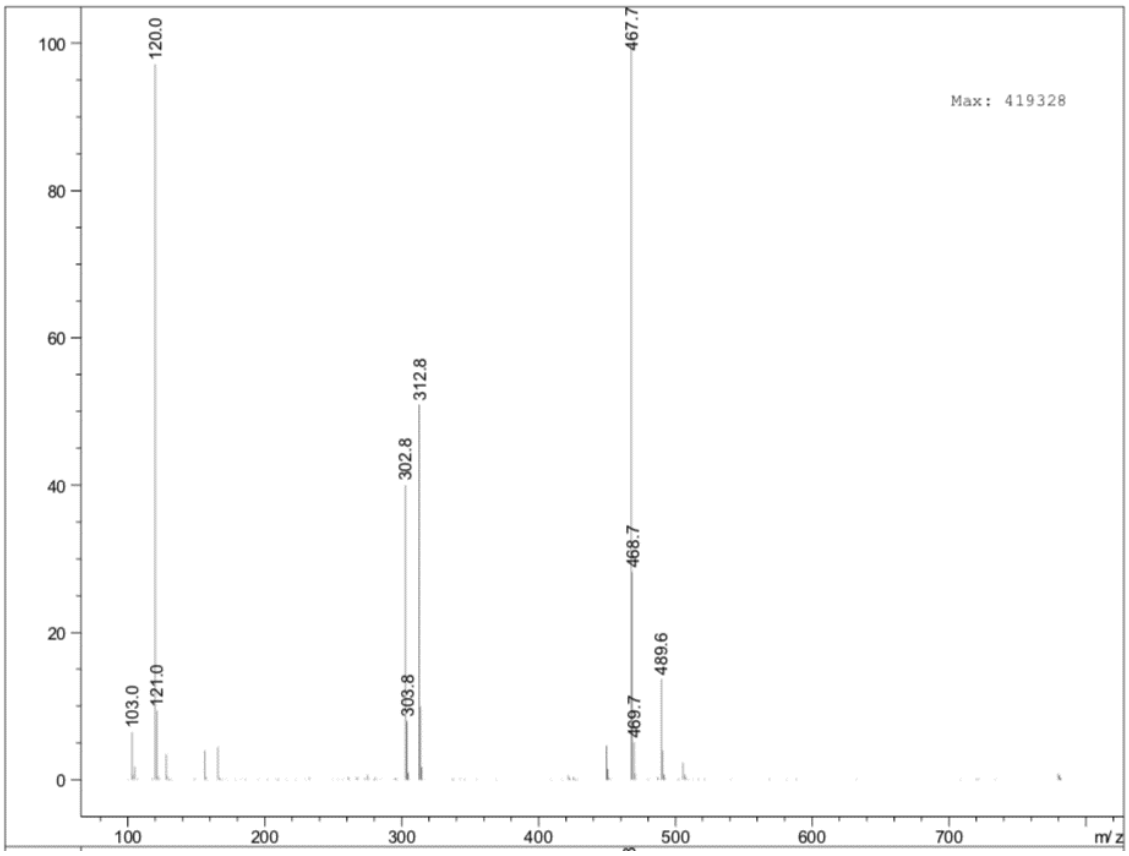

Fig. S16. ESI-MS spectrum of Ac-^{D}Leu-^{L}Phe-^{L}Phe.

S4. ^{1}H-NMR experiment of ^{D}Nle-^{D}Leu-^{L}Phe-^{L}Phe at different temperatures

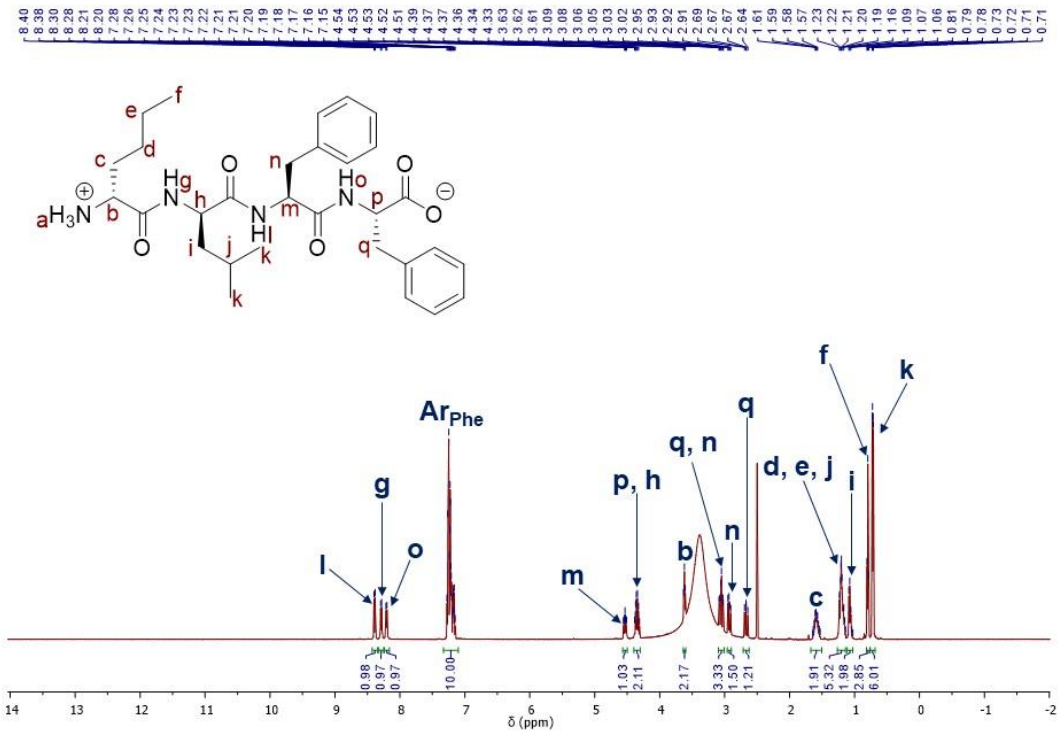

Fig. S17. ^{1}H-NMR spectrum in DMSO-d_6.

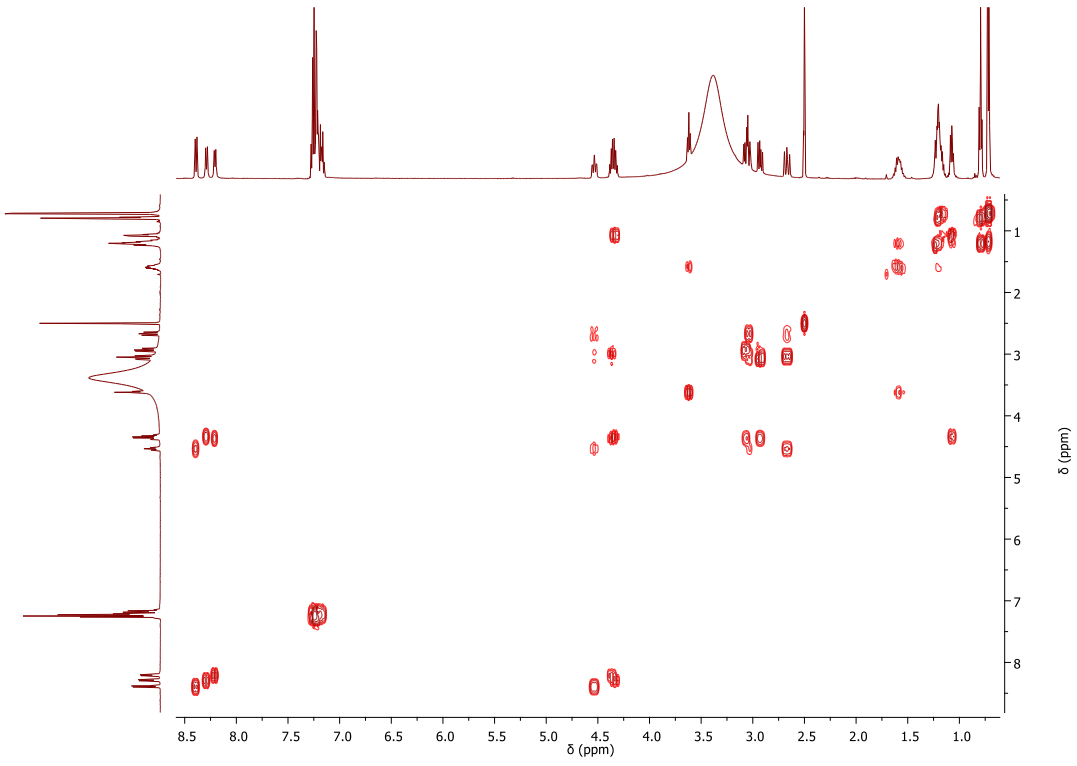

Fig. S18. gCOSY spectrum in DMSO-d_6.

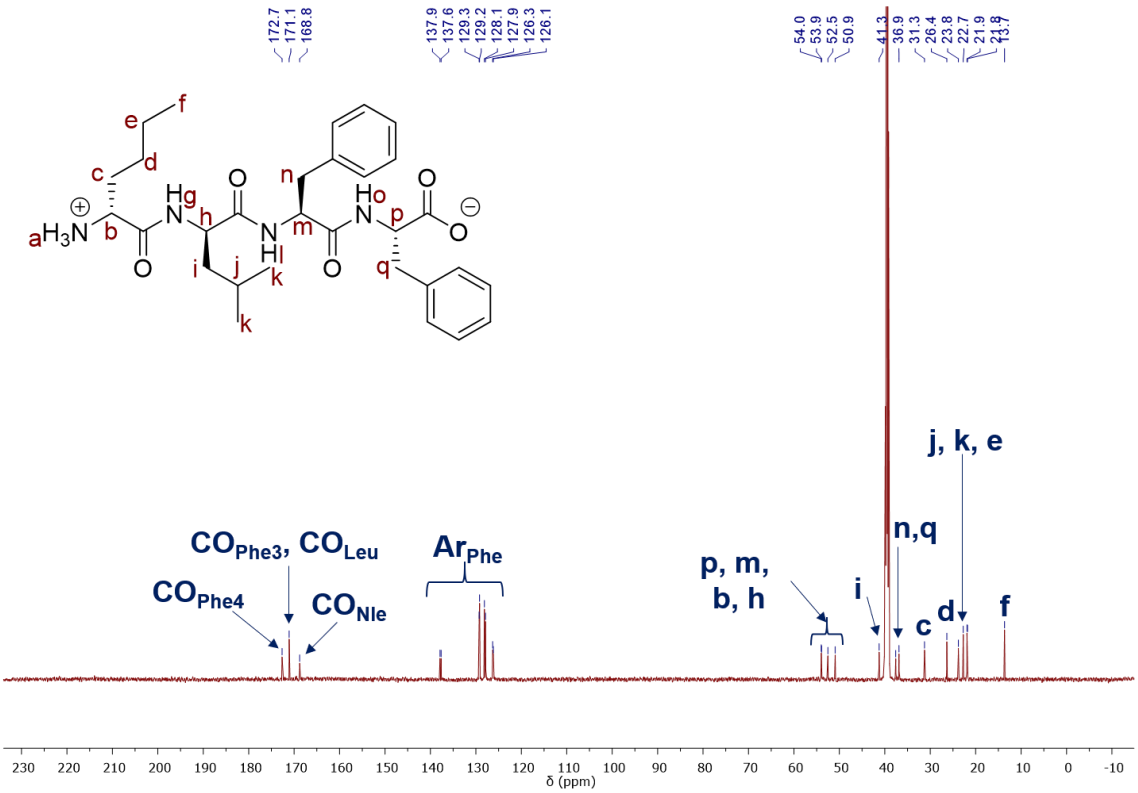

Fig. S19. ^{13}C NMR spectrum in DMSO-d_6.

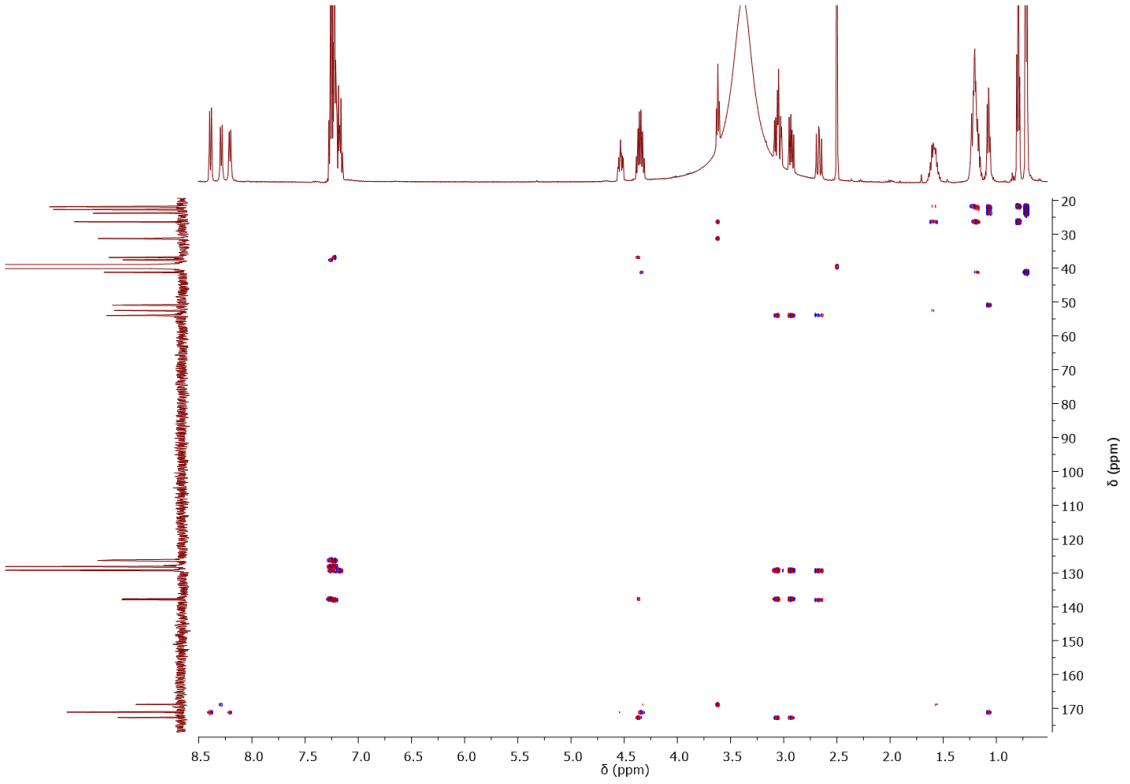

Fig. S20. ^{1}H-^{13}C HMBC spectrum in DMSO-d_6.

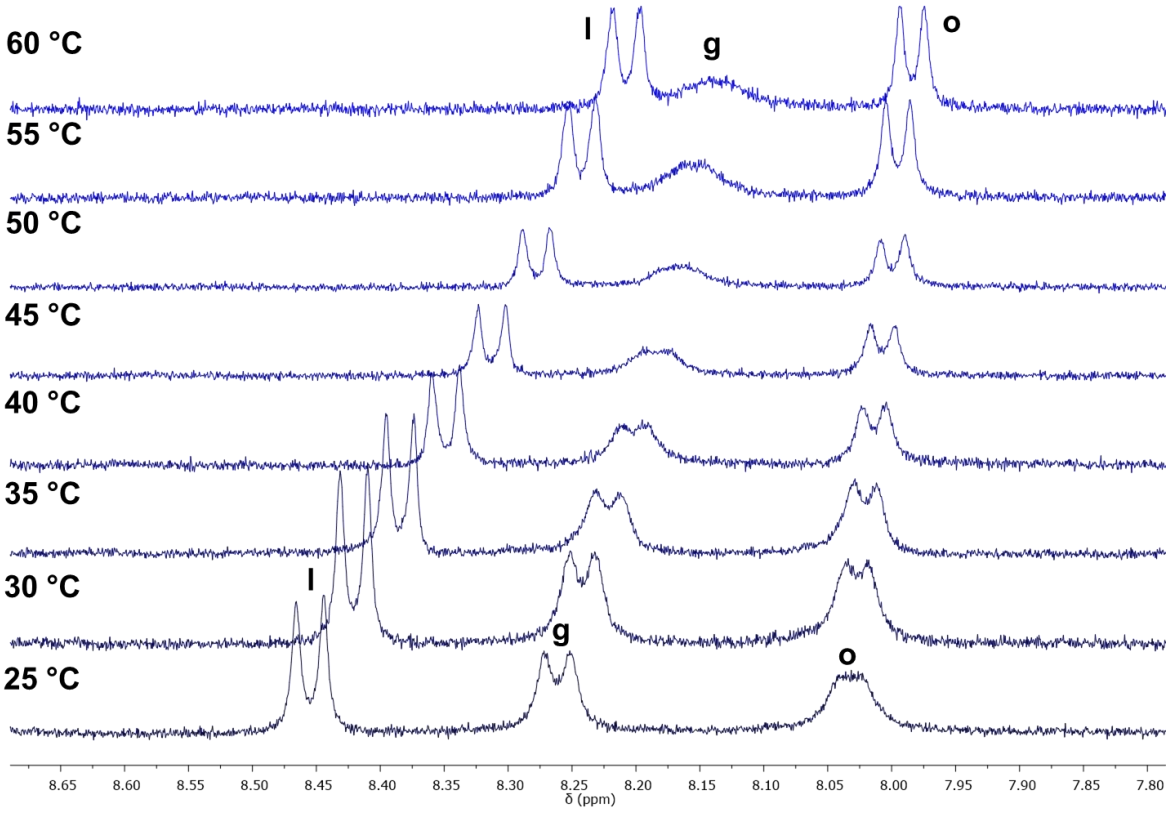

Fig. S21. Amide region of ^{1}H-NMR spectrum of ^{D}Nle-^{D}Leu-^{L}Phe-^{L}Phe at different temperatures (from 25 to 60 °C) in DMSO-d_6.

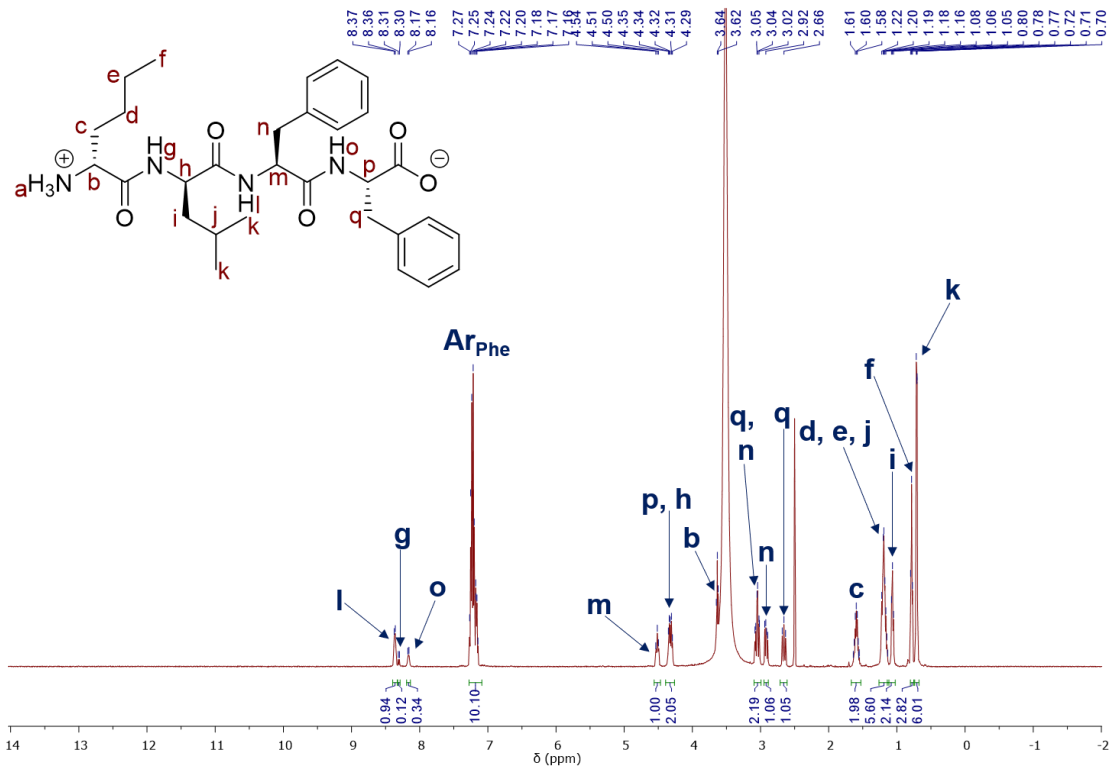

Fig. S22. ^{1}H-NMR spectrum in DMSO-d_6 with 20%water.

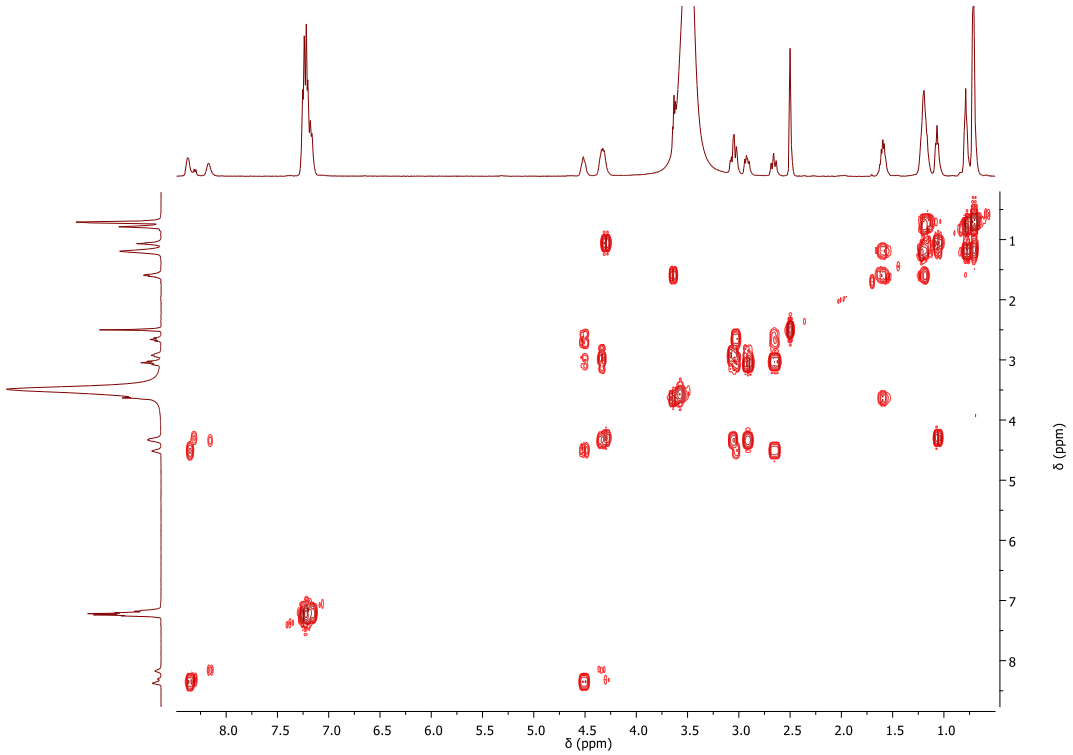

Fig. S23. gCOSY spectrum in DMSO-d_6 with 20% water.

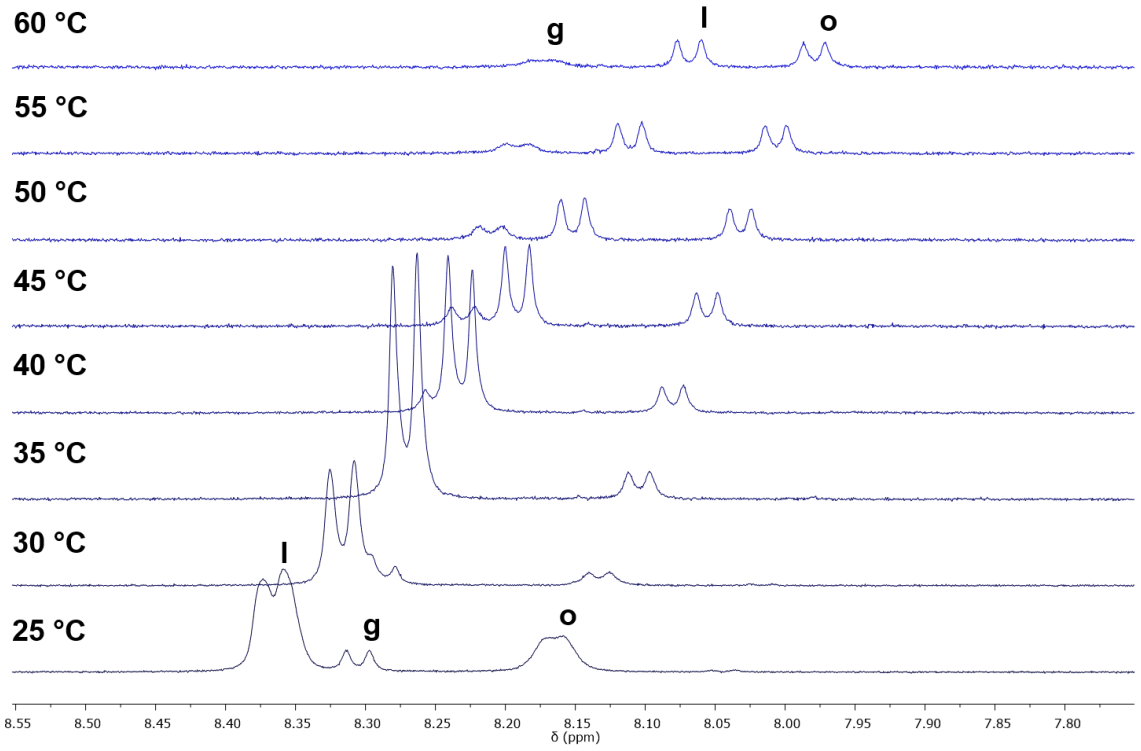

Fig. S24. Amide region of ^{1}H-NMR spectrum of ^{D}Nle-^{D}Leu-^{L}Phe-^{L}Phe at different temperatures (from 25 to 60 °C) in DMSO-d_6 with 20% water.

S5. ^{1}H-NMR experiment of ^{L}Nle-^{L}Leu-^{L}Phe-^{L}Phe at different temperatures

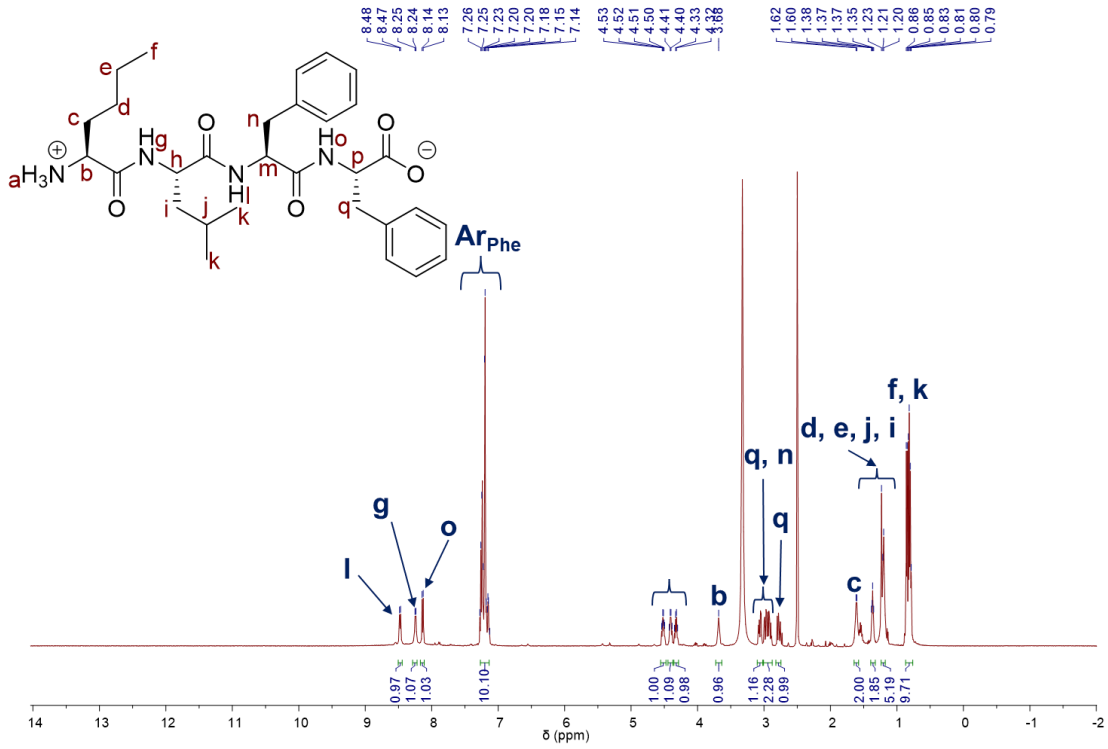

Fig. S25. ^{1}H-NMR spectrum in DMSO-d_6.

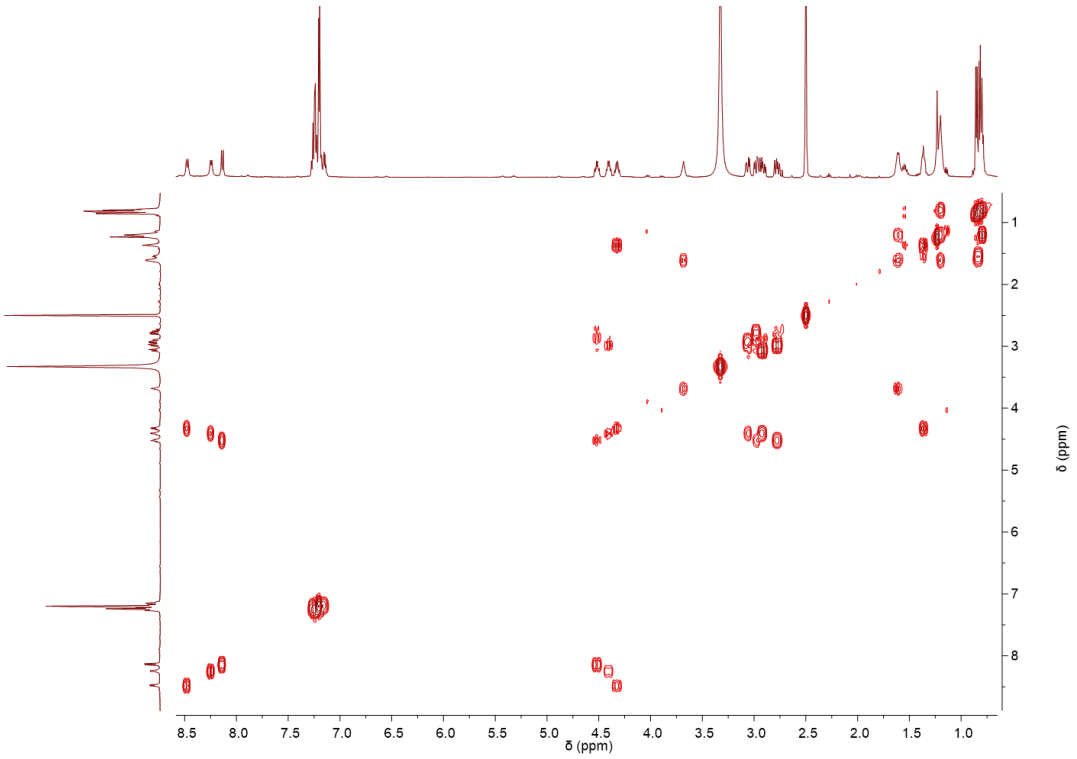

Fig. S26. gCOSY spectrum in DMSO-d_6.

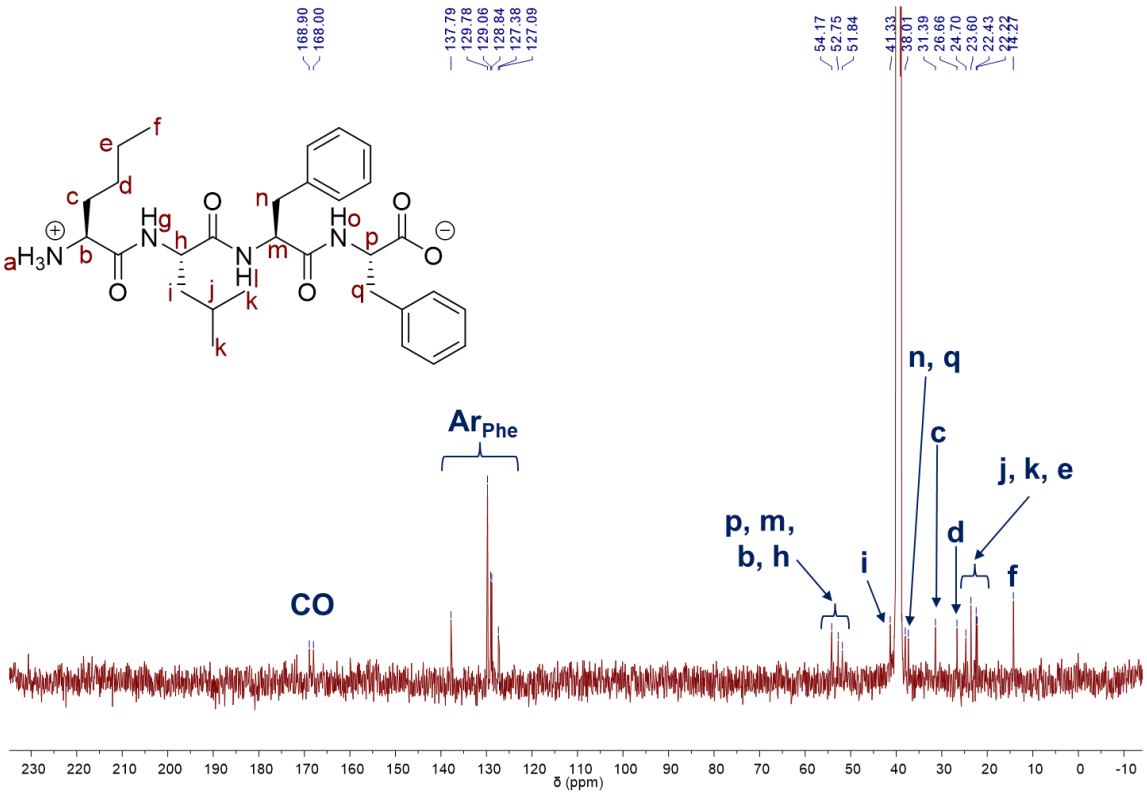

Fig. S27. ^{13}C NMR spectrum in DMSO-d_6.

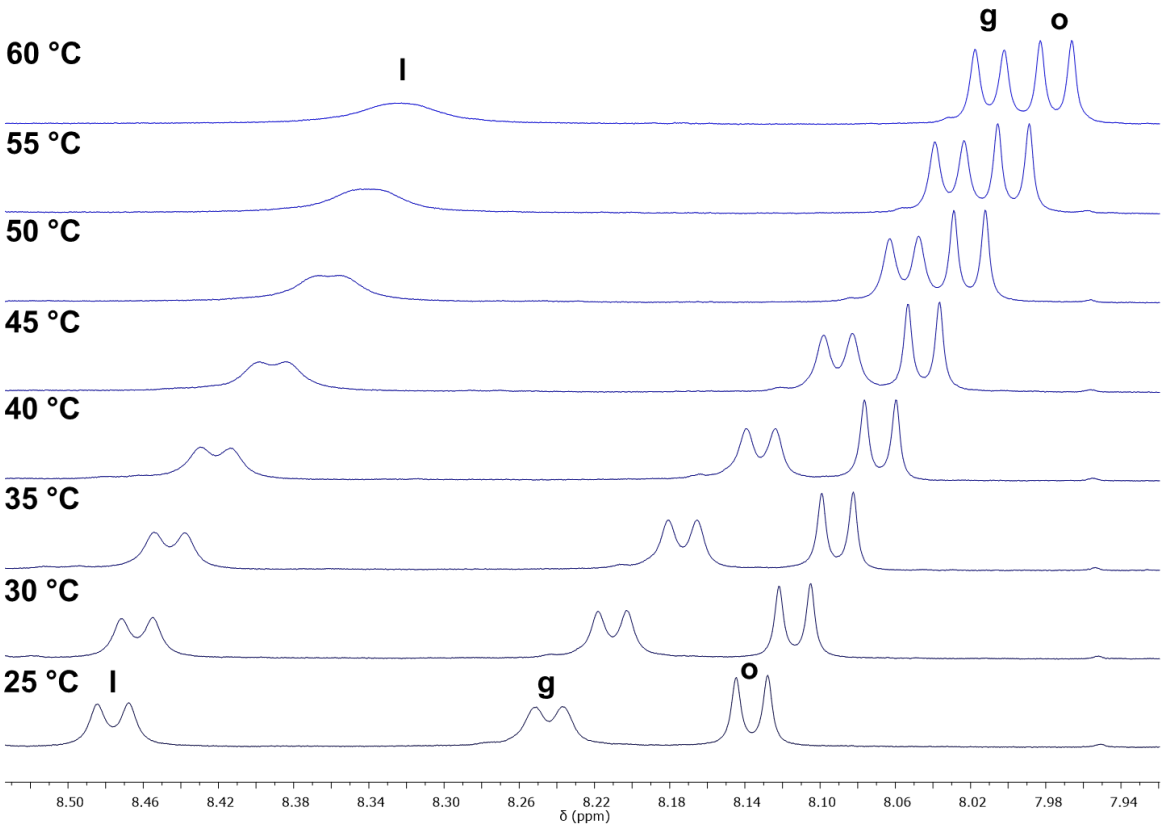

Fig S28. Amide region of ^{1}H-NMR spectrum of ^{L}Nle-^{L}Leu-^{L}Phe-^{L}Phe at different temperatures (from 25 to 60 °C) in DMSO-d_6.

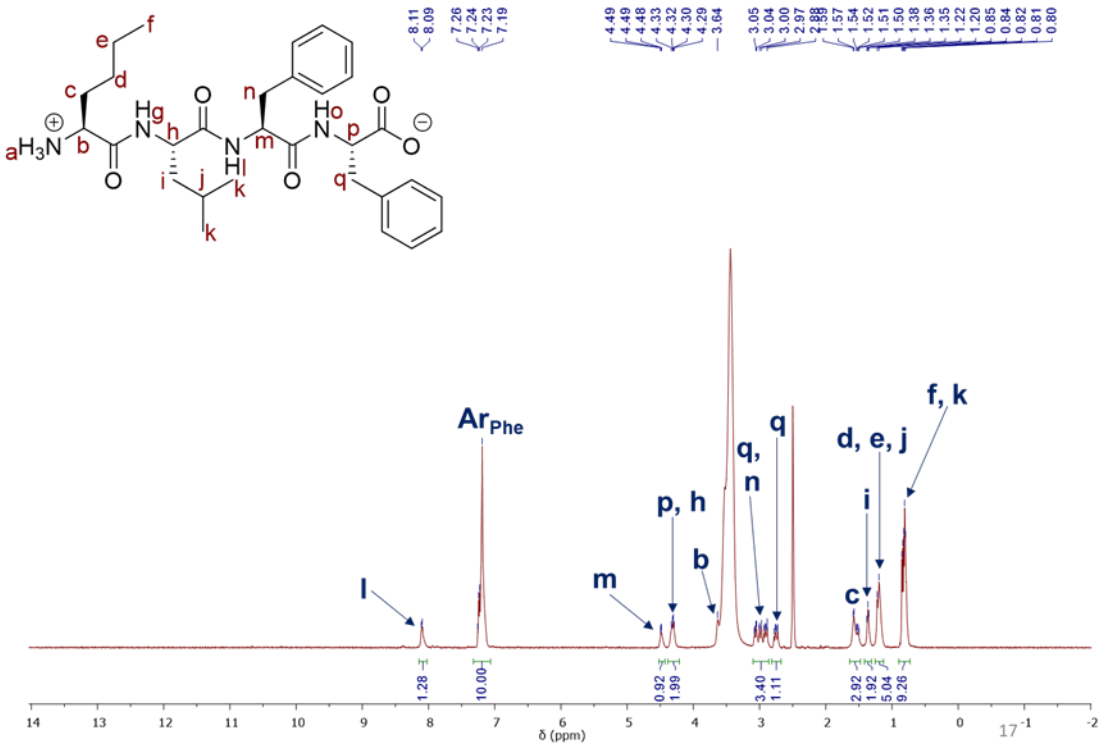

Fig. S29. ^{1}H-NMR spectrum in DMSO-d_6 with 20%water.

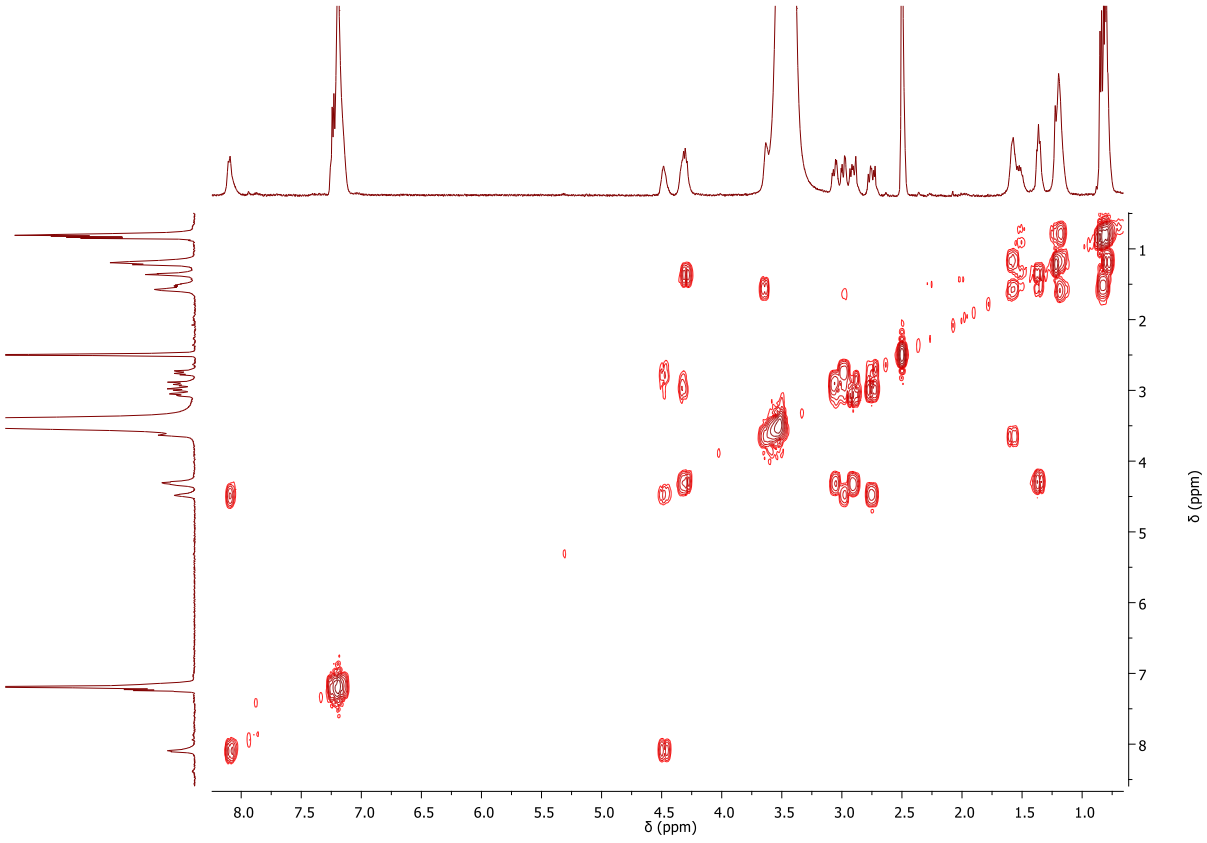

Fig. S30. gCOSY spectrum in DMSO-d_6 with 20% water.

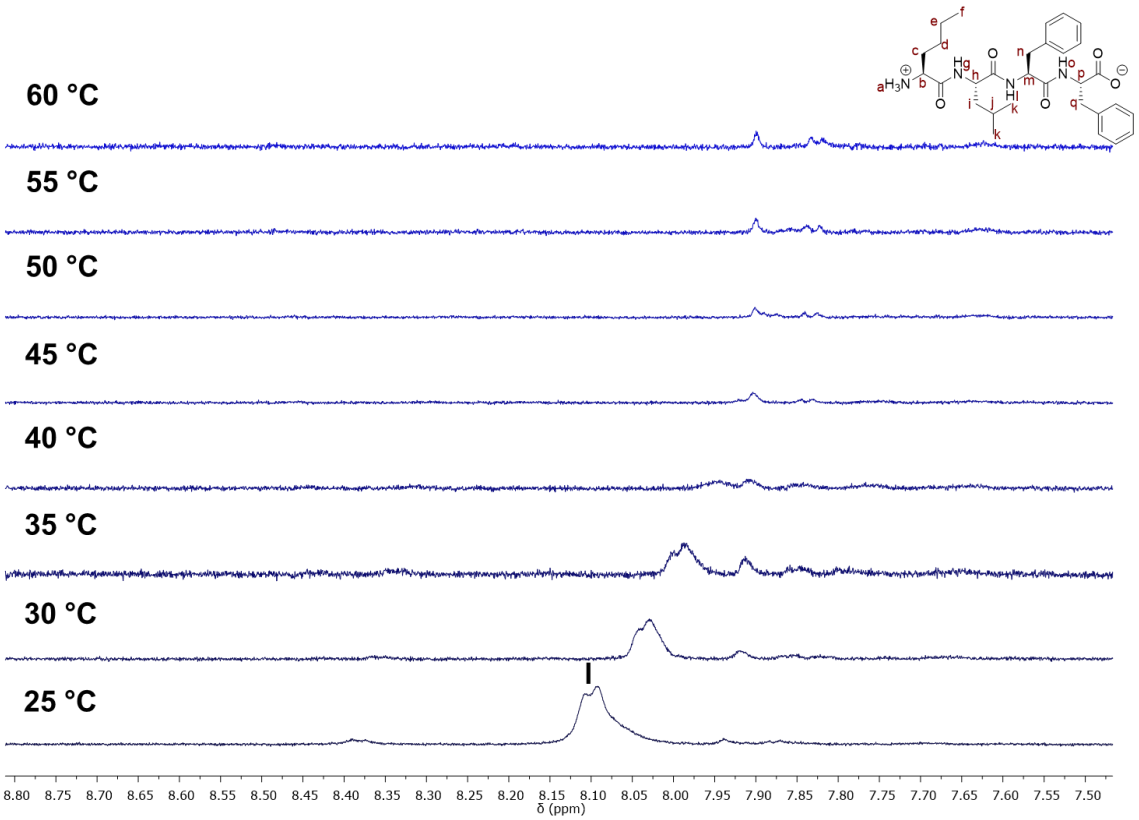

Fig. S31. Amide region of ^{1}H-NMR spectrum of ^{L}Nle-^{L}Leu-^{L}Phe-^{L}Phe at different temperatures (from 25 to 60 °C) in DMSO-d_6 with 20% water.

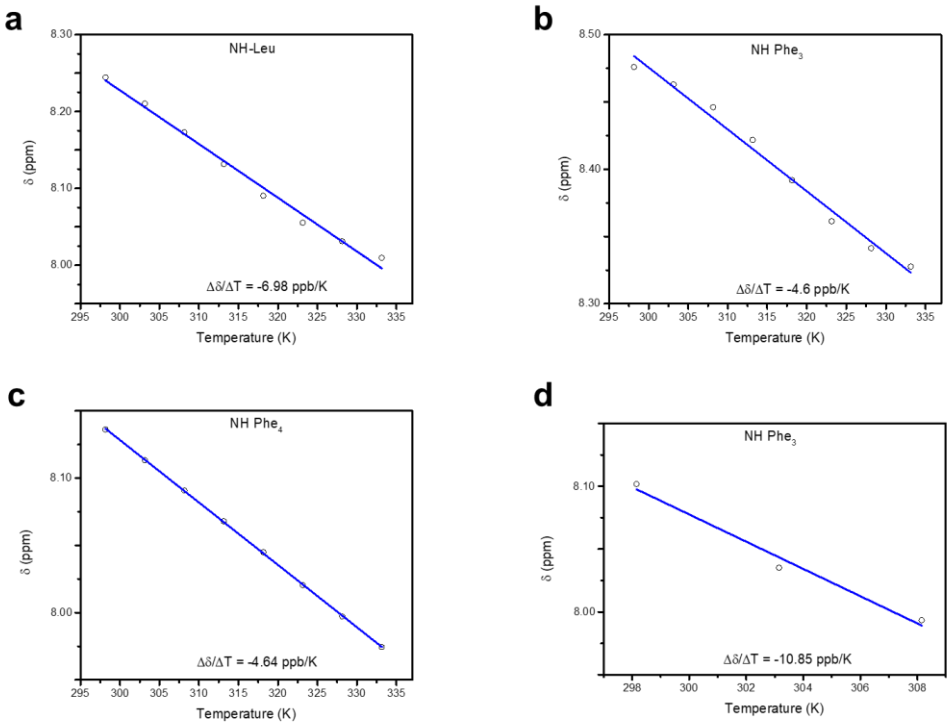

Fig. S32. Intramolecular H-bonds in the homorochiral tetrapeptide. Variable-temperature ^{1}H-NMR analysis of CONH signals in DMSO (a-c) and with 20% water (d). Note: higher amounts of water led to precipitation.

S6. MD data

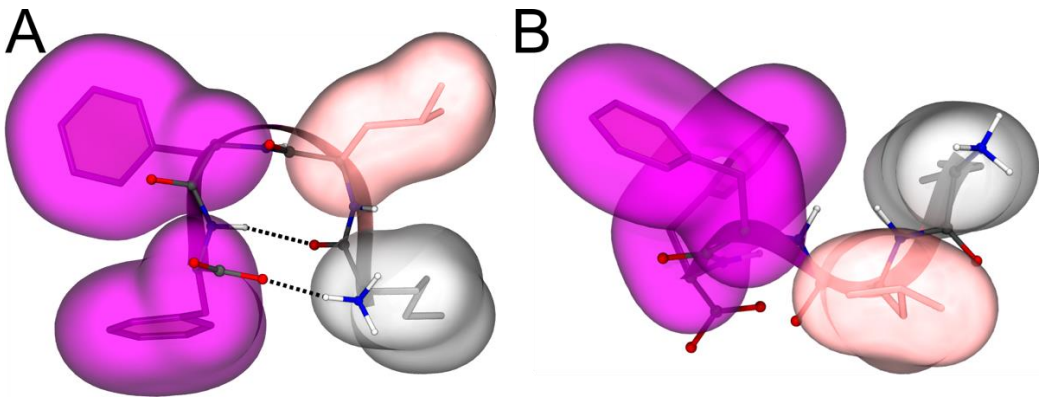

Fig. S33. Most sampled hetero- (A) and homo-chiral (B) conformations along the MD trajectories.

Tetrapeptide	Temperature	Turn conformation* [%]
homochiral	298 K	6.4
	363 K	12.0
heterochiral	298 K	13.8
	363 K	13.5

*Estimated on the basis of the □ and □ angles of the 2nd and 3rd residues of the tetrapeptide (the only ones for which both angles can be calculated).

Table S1. Secondary structure analysis of single tetrapeptide MD simulations. Note that only turns were detected, so the table reports their percentage only.

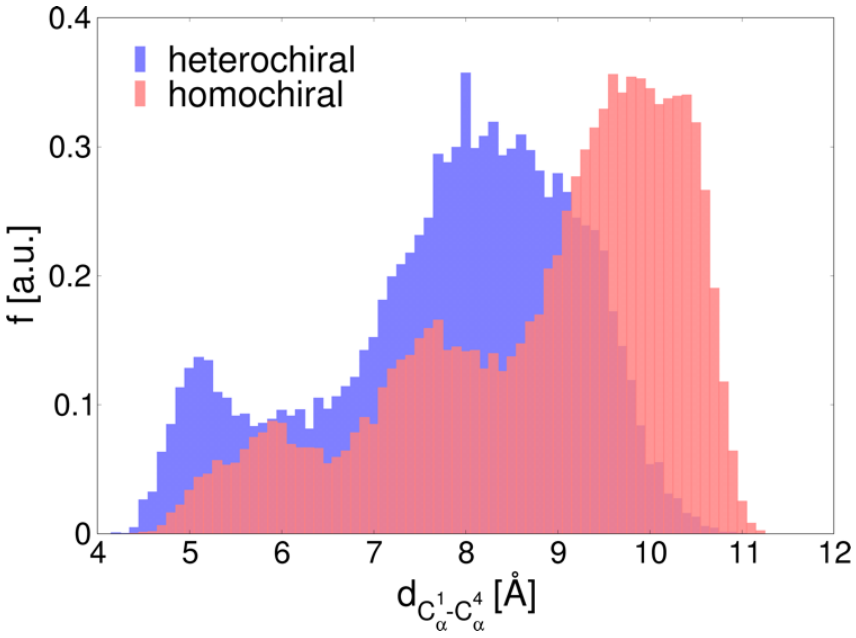

Fig. S34. End-to-end backbone distance distributions calculated for the hetero- and homo-chiral tetrapeptides studied here.

H-bond		Hetero-chiral peptide		Homo-chiral peptide	
Acceptor	**Donor**	**% 298 K**	**% 363 K**	**% 298 K**	**% 363 K**
CO Phe_4	NH Nle_1	9.9	12.4	2.2	2.5
CO Nle_1	NH Phe_4	2.0	2.0	0.7	0.8
CO Leu_2	NH Phe_4	1.8	2.4	1.8	3.3
CO Nle_1	NH Phe_3	1.0	2.0	2.4	2.7
CO Phe_4	NH Leu_2	0.1	0.1	0.0	0.0
CO Phe_3	NH Nle_1	0.1	0.2	0.1	0.0
Total		**15.0**	**19.1**	**7.1**	**9.3**

Table S2. Statistics of H-bond formation. The H-bonds are sorted according to the frequency of formation along the MD simulation of the hetero-chiral peptide at room temperature.

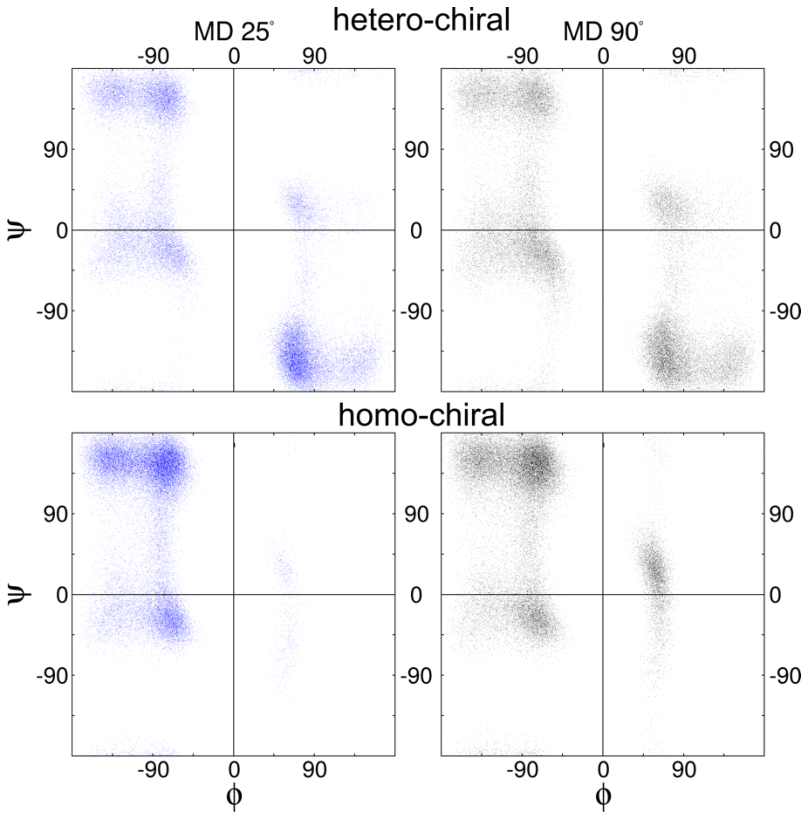

Fig. S35. Ramachandran plot for residues 2 and 3 in the conformations visited by the heterochiral (top) and homochiral (bottom) tetrapeptides during the MD at 298 K (25 °C, left) and 363 K (90 °C, right).

	At RT before heating *(fibril-like)*	At RT after heating *(plate-like)*	Δ
Average RMSF [Å]	18.4 ± 19.3	12.6 ± 17.7	-6.3
% aa with RMSF < 10 Å	63.6 ± 5.2	80.8 ± 11.8	+17.2
% aa with RMSF < 5 Å	8.8 ± 6.9	62.7 ± 27.6	+53.8

Table S3. System rigidification upon heating to 363 K and subsequent cooling to 298 K. Root Mean Square Fluctuation (RMSF) of tetrapeptides estimated along 5 independent MD simulations at 298 K before and after heating to 363 K. The average RMSF as well as the percentages of aa displaying an RMSF lower than 10 or 5 Å are reported. Calculations were performed over the last 100 ns (500 frames) of each simulation. Despite the non-small standard deviations, there is a clear trend showing rigidification of the system due to the release of water molecules from the surface of the peptides. The higher compaction and increased energetic stability of the assembly of tetrapeptides lead also to a consistent reduction in the fluctuations of the solute, and in particular to an increase in the percentage of residues displaying low to medium RMSF values.

MD replica	**298 K before heating [nm^2]**	**298 K after cooling [nm^2]**	**[%]**
1	1477 (23)	1290 (15)	-13
2	1467 (19)	1204 (15)	-18
3	1467 (23)	1184 (17)	-19
4	1369 (32)	1040 (23)	-24
5	1437 (18)	909 (12)	-37
Average	**1443 (22)**	**1125 (75)**	**-22 (5)**

Table S4. Variation in the Solvent Accessible Surface Area (SASA) during MD simulations of heterochiral peptides' self-assembly. See caption of Table S3 for more details.

	MD replica	298 K before heating [#]	298 K after cooling [#]	Δ [%]
Peptide-peptide	1	685 (19)	854 (23)	25
	2	682 (17)	850 (18)	25
	3	687 (20)	909 (17)	32
	4	658 (21)	920 (19)	40
	5	651 (23)	968 (20)	49
	Average	**673 (8)**	**900 (25)**	**34 (5)**
Peptide-water	1	3525 (50)	3035 (40)	-14
	2	3474 (45)	2984 (37)	-14
	3	3510 (49)	2911 (40)	-17
	4	3726 (44)	3057 (34)	-18
	5	3568 (41)	3015 (37)	-15
	Average	**3561 (49)**	**3000 (28)**	**-16 (1)**
Water-bridged	1	509 (16)	477 (19)	-6
	2	486 (15)	515 (17)	6
	3	510 (17)	484 (18)	-5
	4	531 (18)	522 (16)	-2
	5	509 (19)	522 (17)	3
	Average	**509 (8)**	**504 (11)**	**-1 (3)**

Table S5. Variation in the number of peptide-peptide, peptide-solvent, and peptide-water-peptide H-bonds during MD simulations of heterochiral peptides' self-assembly. See caption of Table S3 for more details.

S7. ^{D}Nle-^{D}Leu-^{L}Phe-^{L}Phe self-assembly

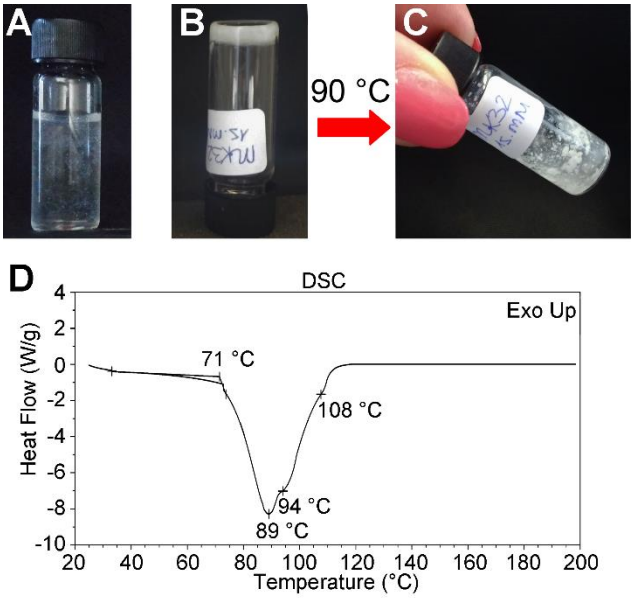

Figure S36. A. Visible fibrillization occurred at 0.05 % wt. **B.** Self-supporting hydrogel at 0.67 % wt. **C.** Peptide aggregation upon heating to 90 °C. **D.** DSC data for the hydrogel.

S8. Photographs of ^{L}Nle-^{L}Leu-^{L}Phe-^{L}Phe solution and aggregates

Figure S37. Left: Solution at 0.05 % wt. Right: Aggregates at 0.67 % wt.
Analogous data were obtained for *N*-acetylated ^{D}Leu-^{L}Phe-^{L}Phe.

S9. *In vitro* cytotoxicity assay

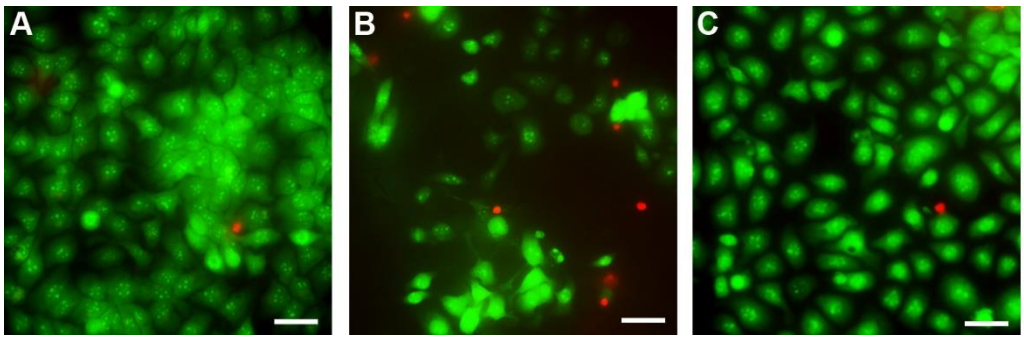

Figure S38. Lie/dead assays, from left to right: control, homochiral and heterochiral tetrapeptides.

S10. Protease assay data

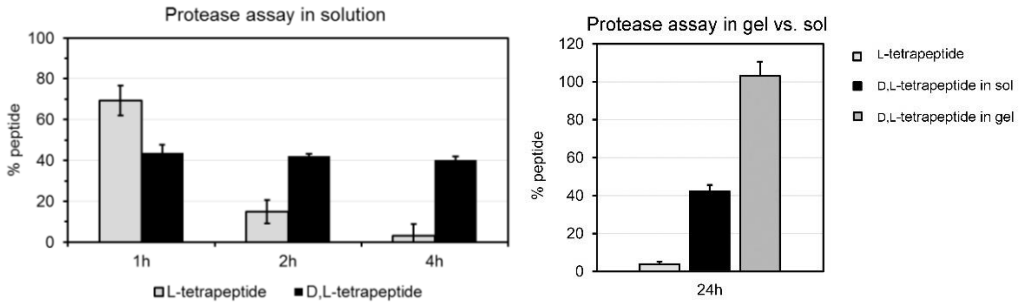

Figure S39. Protease assay of peptides in solution and hydrogel.

S11. CD spectra of ^{D}Nle-^{D}Leu-^{L}Phe-^{L}Phe over a heating ramp up to 85 °C

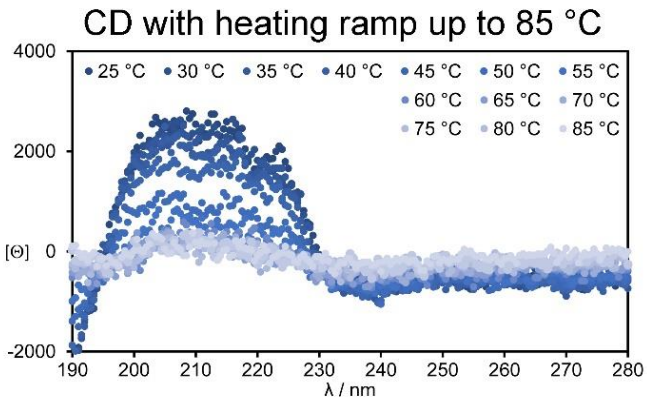

Fig. S40. Circular dichroism spectra of the D,L-tetrapeptide hydrogel fibrils over a heating ramp from RT to 85 °C. The spectra intensity decreases gradually upon heating, thus indicating loss of secondary structure. No shift was observed to suggest a change from one secondary structure to another.

S12. Single-crystal XRD data (CCDC2347110)

The peptide was crystallised in DMSO as a zwitterion. The asymmetric unit contains one molecule of peptide, no solvent molecules are present in the crystal. The peptide crystallises in a *P2* monocline unit cell, with a total of four molecules in the unit cell (Fig. S41).

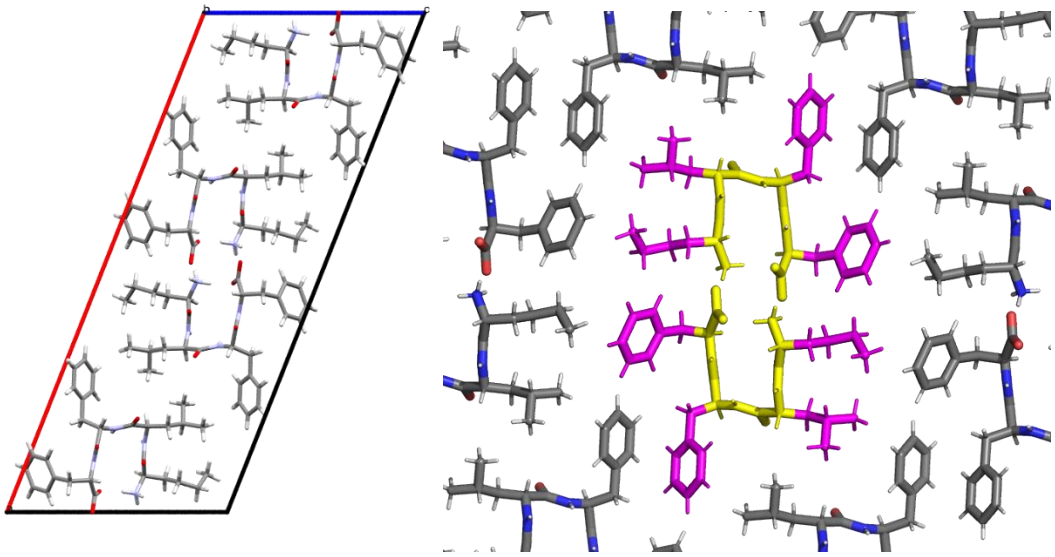

Fig. S41: A: Unit cell of the crystal of D-Nle-D-Leu-L-Phe-L-Phe, represented along the *b* crystallographic axis, with stick representation. Black: carbon, blue: nitrogen, red: oxygen, white: hydrogens. **B:** Crystal packing viewed along the *b* crystallographic axis. Purple: side chains, yellow: backbone.

The non-covalent interactions present in the crystal packing are Van der Waals forces and hydrogen bonds (Figs. S41B, S42). All the side chains of the peptide are involved in hydrophobic interactions but no intra- or inter-molecular π-π stacking can be clearly distinguished. The peptide backbone is involved in several hydrogen bond interactions. Leucine and phenylalanine amide nitrogen atoms form two hydrogen bonds, respectively, with the leucine and phenylalanine carbonyl oxygen atoms of a neighbouring molecule, the only two hydrogen bond interactions below 3.4 Å present in the structure excluding the C and N termini interactions (Figure S42A). C and N-termini form intra- and inter-molecular salt-bridge interactions (Figure S42B, C), with the C-terminus of a peptide bridging between two N-termini of neighbouring peptides, and similarly the N-terminus between two C-termini. The zwitterion form of the peptide crystallised without solvent in the crystal packing.

Crystallographic details.

A plate-shaped single crystal of the peptide was collected with a loop, cryoprotected by dipping the crystal in an oil-based cryoprotectant, namely Parabar 10312 (previously known as Paratone N, from Hampton Research). The crystal was mounted on the diffractometer at the synchrotron Elettra, Trieste (Italy), beamline XRD1. Temperature was kept at 100 K by a stream of nitrogen on the crystal. Diffraction data were collected by the rotating crystal method using synchrotron radiation, wavelength 0.70 Å, rotation interval 0.5°/image, crystal-to-detector distance of 85 mm. A total of 720 images were collected to increase redundancy of data. Reflections were indexed and integrated using the XDS package [1], space group P2 was determined using POINTLESS [2] and the resulting data set was scaled using AIMLESS [3]. Phase information were obtained by direct methods using the software SHELXT [4]. Refinements cycles were conducted with SHELXL [5], operating through the ShelXLe GUI [6], by full-matrix least-squares methods on F2. Unit cell parameters and scaling statistics are reported in Table S6. The asymmetric unit contains a molecule of the peptide. Hydrogen atoms of the peptide were added at geometrically calculated positions and refined isotropically, with thermal parameters dependent on those of the attached atom. All the atoms within the asymmetric unit, except the hydrogen atoms, have been refined with anisotropic thermal parameters. Refinement statistics are reported in Table S6.

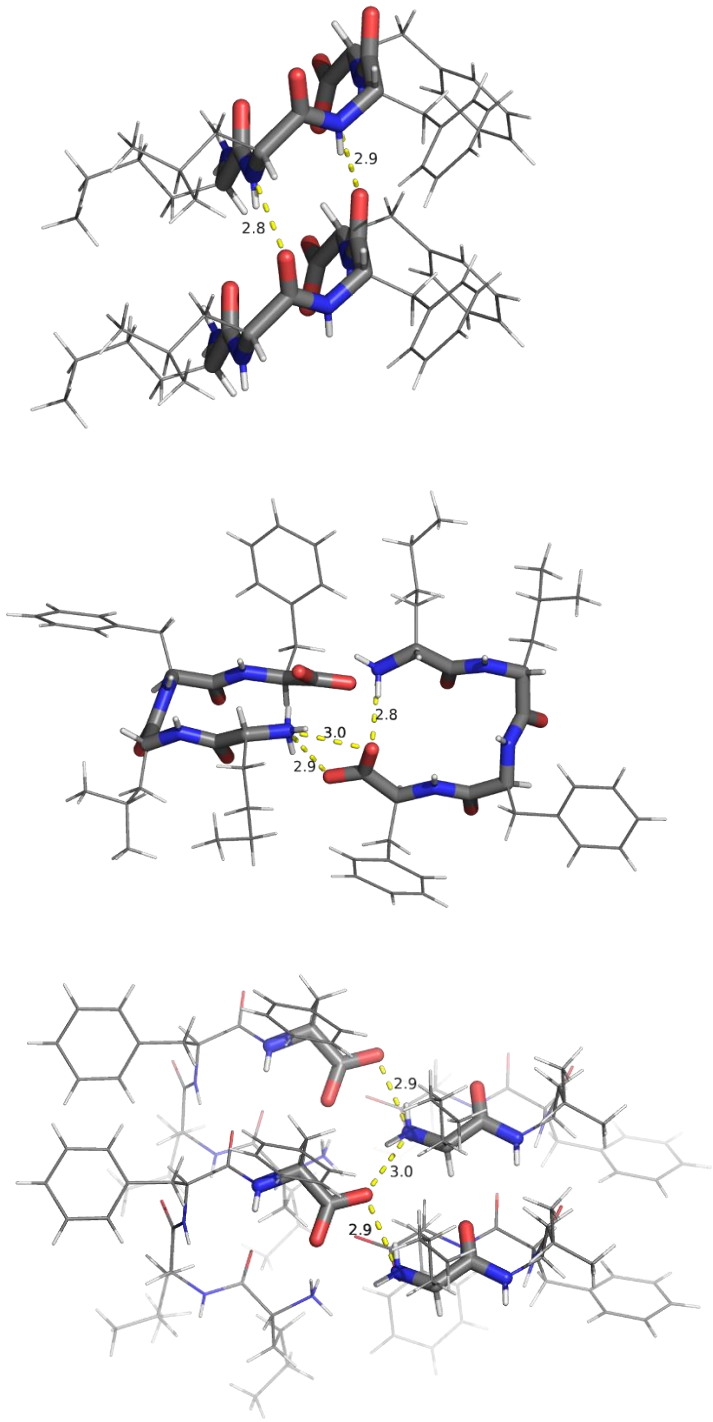

Figure S42: A: hydrogen bonds between the backbone amide nitrogen atoms of a peptide and the carbonyl oxygen atoms of a neighbouring peptide. **B and C**: salt-bridge interactions between C and N-termini. The backbone atoms are represented as sticks, while a wire repsentation is used for side chains, for clarity. In panel C, the stick representation is used only for the backbone of the N and C-terminal residues.

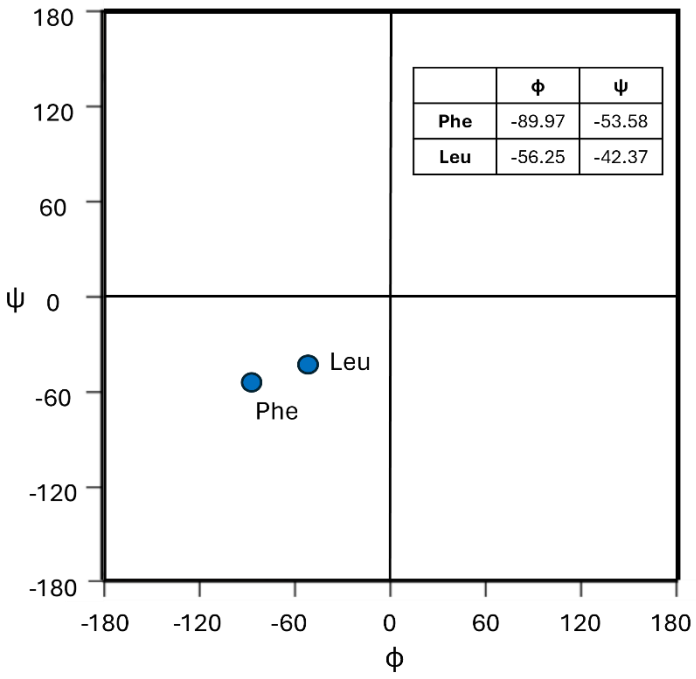

Figure S43: Ramachandran plot of D-Nle-D-Leu-L-Phe-L-Phe backbone torsion angles, as displayed by the software COOT.

	D-Nle-D-Leu-L-Phe-L-Phe
Formula	$C_{30}\,H_{42}\,N_4\,O_5$
Temperature (K)	100
Wavelength (Å)	0.7
Crystal system	Monoclinic
Space group	*P 2*
a (Å)	38.128(8)
b (Å)	5.1770(10)
c (Å)	15.602(3)
α (°)	90
β (°)	111.48(3)
γ (°)	90
V (Å^3)	2865.8(11)
Z, ρcalc (g/cm^3)	4, 1.249
μ (mm^{-1})	0.053
F (000)	1160
Data collection θ range	1.13 – 20.467
Refl. Collected / unique	9907 / 2897
Rint	0.1292
Completeness (%)	97.8
Data/Restraints/Parameters	2897 / 0 / 357
GooF	1.066
R1, wR2 [I>2σ(I)]	0.0881 / 0.2329
R1, wR2 all data	0.1376 / 0.2675

Table S6: Crystallographic data for D-Nle-D-Leu-L-Phe-L-Phe.

S14. References

[1] Kabsch, W. Acta Crystallogr., Sect. D. 2010, 66, 125−132.

[2] Evans, P. R. Acta Crystallogr., Sect. D. 2006, 62, 72−82.

[3] Evans, P. R., Murshudov, G. N. Acta Crystallogr., Sect. D. 2013, 69, 1204−14.

[4] Sheldrick, G. M. Acta Crystallogr., Sect. A. 2008, 64(Pt 1), 112-22.

[5] Sheldrick, G. M. Acta Crystallogr., Sect. C. 2015, 71, 3–8.

[6] Hübschle, C. B. et al. J. Appl. Cryst., 2011, 44, 1281-1284.